Insights into (U)HP metamorphism of the Western Gneiss Region, Norway: A high-spatial resolution and high-precision zircon study

Joel W. DesOrmeau and Stacia M. Gordon, Department of Geological Sciences, University of Nevada Reno, Nevada, USA

Andrew R.C. Kylander-Clark and Bradley R. Hacker, Department of Earth Science, University of California, Santa Barbara, California, USA

Samuel A. Bowring, Department of Earth, Atmospheric, and Planetary Sciences, Massachusetts Institute of Technology, Cambridge, Massachusetts, USA

Blair Schoene and Kyle M. Samperton, Department of Geosciences, Princeton University, Princeton, New Jersey, USA

Corresponding author: J.W. DesOrmeau, Department of Geological Sciences, 1664 N. Virginia St. MS0172, University of Nevada Reno, Reno, NV 89557, USA (desormeau@nevada.unr.edu)

Key words

Zircon; Laser ablation split-stream; Isotope dilution–thermal ionization mass spectrometry; Norway; Ultrahigh-pressure metamorphism

Abstract

Combining high-spatial resolution and high-precision geochronology and geochemistry of zircon provides constraints on the timing and duration of ultrahigh-pressure (UHP) metamorphism resulting from the collision of Baltica–Avalonia and Laurentia during the Scandian orogeny in the Western Gneiss Region of Norway. Zircons were extracted from a layered eclogite in the Saltaneset region (southern UHP domain) and from an eclogite in the Ulsteinvik region (central UHP domain). Zircons were first analyzed for U-Pb and trace element compositions by laser ablation split-stream (LASS) inductively coupled plasma mass spectrometry (ICP-MS), followed by analysis of those same zircons that yielded Scandian dates by integrated U-Pb isotope dilution–thermal ionization mass spectrometry and Trace Element Analysis (TIMS-TEA). LASS results from a garnet–quartz layer within the Saltaneset eclogite give Scandian dates of ca. 413–397 Ma, with subsequent ID-TIMS analyses ranging from 408.9 ± 0.4 Ma to 401.4 ± 0.2 Ma (2σ). An omphacite-rich layer from the same eclogite yields LASS dates of ca. 414–398 Ma and a single ID-TIMS date of 396.7 ± 1.4 Ma. In comparison, the Ulsteinvik eclogite LASS results give dates spanning ca. 413–397 Ma, whereas ID-TIMS analyses range from 409.6 ± 0.6 Ma to 401.3 ± 0.4 Ma. ID-TIMS zircon data from the eclogites reveals two age populations: 1) ca. 409–407 Ma and 2) ca. 402 Ma. Both *in situ* and solution trace element data show a distinct pattern for Scandian zircons, with strongly-depleted HREE and weakly-negative Eu anomalies (Eu/Eu*), whereas inherited zircon REE patterns are distinguished by steep HREE slopes and marked negative Eu/Eu*. When coupled with partition coefficients calculated for zircon and garnet, these REE patterns indicate that zircon (re)crystallized during eclogite-facies metamorphism at ca. 409–407 Ma and ca. 402 Ma at two widely separated UHP localities.

1. Introduction

The Western Gneiss Region (WGR) of western Norway is one of the largest and best-exposed ultrahigh-pressure (UHP) terranes on Earth. Because of this, the WGR has been extensively studied to better understand the geodynamics of subduction and subsequent exhumation of 30,000 km^2 (5,000 km^2 of which are UHP rocks) of continental crust (e.g., Krogh et al., 1974, 2011; Krogh, 1977, 1982; Lappin and Smith, 1978; Griffin and Brueckner, 1980, 1985; Austrheim, 1987; Tucker et al., 1990; Andersen et al., 1991; Wain, 1997; Cuthbert et al., 2000; Wain et al., 2000; Terry et al., 2000a, 2000b; Root et al., 2005; Hacker, 2007; Kylander-Clark et al., 2009; Hacker et al., 2010). Since the initial discovery of a coesite-eclogite province in the southern WGR (Smith, 1984, 1988), thermobarometry and identification of microdiamonds, coesite, and polycrystalline quartz grains within eclogite and quartzofeldspathic gneiss has aided in the recognition of three separate UHP domains (Root et al., 2005): the southern (Nordfjord), central (Sørøyane), and northern (Nordøyane) domains (Fig. 1a) (e.g., Dobrzhinetskaya et al., 1995; Wain, 1997; Cuthbert et al., 2000; Terry et al., 2000a; Wain et al., 2000; Carswell and Cuthbert, 2003; Carswell et al., 2003a; Walsh and Hacker, 2004; Young et al., 2007; Butler et al., 2013; Smith and Goddard, 2013).

A general increase in peak UHP pressure and temperature (*P–T)* to the northwest across the WGR points to the coherent nature of the terrane during subduction and exhumation from mantle depths (e.g., Krogh, 1977; Lappin and Smith, 1978; Griffin et al., 1985; Andersen et al., 1991; Cuthbert et al., 2000; Carswell and Cuthbert, 2003; Carswell et al., 2006; Hacker et al., 2010). Characterizing the processes involved in the deep subduction and exhumation of such a large tract of continental crust requires a detailed understanding of the timescales of peak UHP metamorphism (e.g., Terry et al., 2000b; Carswell et al., 2003a, 2003b; Root et al., 2004; Kylander-Clark et al., 2007, 2009; Krogh et al., 2011).

Some (U)HP terranes were likely at mantle depths for tens of millions of years prior to exhumation (Kylander-Clark et al., 2012). This was first recognized in the Dabie Shan of China (Hacker et al., 1998), and then in the WGR of Norway (Kylander-Clark et al., 2008), where geochronological data suggests (U)HP metamorphism from ca. 430–400 Ma (Table 1; Section 2.2). Previous efforts to determine the timing of (U)HP metamorphism in the WGR have relied on techniques that analyze minerals that can be directly linked to the metamorphic evolution of eclogites (e.g., garnet and clinopyroxene) as well as more refractory accessory minerals (e.g., zircon and monazite) (Table 1). However, limitations in some previous geochronological studies of the WGR include: (1) data sets consisting of relatively few analyses (e.g., two-point isochrons); (2) dating of zoned garnet, for which isotopic ages may be averaging dates from multiple, distinct growth zones; (3) dating of multi-grain separates by U-Pb ID-TIMS that may result in inaccurate and/or mixed ages; and (4) ambiguities in how the dated minerals relate to the (U)HP metamorphism. This study builds upon these previous efforts by obtaining U-Pb dates from the same zircon domains via both laser ablation–inductively coupled plasma mass spectrometry (LA-ICP-MS) and from single-grain chemical abrasion–isotope dilution–thermal ionization mass spectrometry (ID-TIMS)—combining a high-spatial resolution technique and a high-precision technique on the same zircon.

In order to interpret geochronological data obtained from eclogites, it is crucial to link dates to different parts of the *P*–*T* path. The trace element composition of zircon can be used as a tool in age interpretations, particularly when coupled with the trace element composition of coexisting garnet. Zircon that (re)crystallizes at high pressure will likely display a flat normalized heavy rare earth element (HREE) pattern (e.g., Lu/Gd ~ < 3), due to the presence of garnet. Moreover, high-pressure zircon may have a flat-to-positive Eu anomaly (e.g., Eu/Eu* > 0.75), indicating (re)crystallization when plagioclase was unstable (Hinton and Upton, 1991; Schaltegger et al., 1999; Hoskin and Ireland, 2000; Rubatto, 2002; Hoskin and Schaltegger, 2003; Rubatto and Hermann, 2003; Rubatto and Hermann, 2007a). In addition, empirically and experimentally determined REE partition coefficients allow assessment of equilibrium between zircon and garnet (e.g., Hinton and Upton, 1991; van Westrenen et al., 1999; Rubatto, 2002; Whitehouse and Platt, 2003; Kelly and Harley, 2005; Harley and Kelly, 2007; Rubatto and Hermann, 2007b; Taylor et al., 2014), an additional test to determine whether zircon (re)crystallized in the presence of garnet.

This study presents new U-Pb zircon dates from two coesite- and polycrystalline quartz-bearing eclogites to further evaluate the timescales of UHP metamorphism within the southern and central WGR. Trace element analyses of zircon provide insight into the *P–T* conditions under which zircon (re)crystallization occurred. The results reveal two separate populations of zircon that (re)crystallized under eclogite-facies conditions at ca. 409–407 Ma and ca. 402 Ma within the Ulsteinvik eclogite of the central UHP domain and the Saltaneset eclogite of the southern UHP domain. These results suggest a UHP metamorphic history for the Ulsteinvik eclogite older than the previously recognized 401.6 ± 1.6 Ma age (multi-grain zircon; Carswell et al., 2003a; Tucker et al., 2004), and a UHP history for the Saltaneset eclogite younger than the previously measured 408.3 ± 6.7 Ma age (Sm-Nd isochron; Carswell et al., 2003b).

2. Geologic Background

2.1 Western Gneiss Region

The autochthonous basement of the WGR, the Western Gneiss Complex (WGC) (Fig. 1), is a polymetamorphic terrane composed mainly of granodioritic–tonalitic intrusive rocks predominantly formed between ca. 1690–1620 Ma (Brueckner, 1972; Carswell and Harvey, 1985; Tucker et al., 1990; Skår et al., 1994; Skår, 2000; Austrheim et al., 2003; Corfu et al., 2013) during the Gothian orogeny (Gaál and Gorbatschev, 1987). The WGC was intruded by mafic magmas at ca. 1470–1450 Ma and ca. 1260–1250 Ma (Austrheim et al., 2003; Tucker et al., 2004; Krogh et al., 2011; Corfu et al., 2013; Beckman et al., 2014). Moreover, a ca. 1000–900 Ma granulite-facies overprint related to the Sveconorwegian orogeny accompanied pluton and dike emplacement and migmatization chiefly southwest of Molde (Brueckner, 1972, 1979; Skår et al., 1994; Austrheim, 2003; Skår and Pederson, 2003; Røhr et al., 2004, 2013; Tucker et al., 2004; Root et al., 2005; Glodny et al., 2008; Kylander-Clark et al., 2008; Krogh et al., 2011; Corfu et al., 2013).

This study focuses on metamorphism of the WGR during the Scandian orogeny, the final stage of the early Paleozoic Caledonian orogeny (Roberts and Gee, 1985; Stephens and Gee, 1989; Roberts, 2003; Brueckner and van Roermund, 2004; Hacker and Gans, 2005: Hacker et al., 2010). The Scandian orogeny included a series of tectonic events: (1) closure of the Iapetus Ocean resulted in thrusting of oceanic and continental allochthons east–southeastward over the autochthonous basement of the WGR from ca. 430–415 Ma (Roberts, 2003; Tucker et al., 2004; Hacker and Gans, 2005); (2) westward continental subduction of the Baltica basement and segments of overlying allochthons beneath Laurentia from ca. 430–400 Ma (Andersen et al., 1991, 1998; Terry et al., 2000a; Bingen et al., 2004; Root et al., 2004, 2005; Kylander-Clark et al., 2007, 2009; Spengler et al., 2009; Krogh et al., 2011); and (3) ca. 400–385 Ma near-isothermal decompression and exhumation of the subducted crust from mantle to shallow crustal depths (Andersen et al., 1998; Tucker et al., 1990, 2004; Terry et al., 2000a; Schärer and Labrousse, 2003; Walsh and Hacker, 2004; Root et al., 2005; Hacker, 2007; Kylander-Clark et al., 2008; Krogh et al., 2011; Gordon et al., 2013; Spencer et al., 2013; Kylander-Clark and Hacker, 2014).

The Scandian collision between Laurentia and Baltica–Avalonia produced an extensive area (30,000 km^2) of (U)HP eclogites that record *P-T* conditions of 1.5–3.9 GPa and 600–820 ºC (Krogh, 1977, 1982; Lappin and Smith; 1978; Griffin et al., 1985; Cuthbert and Carswell, 1990; Wain, 1997; Cuthbert et al. 2000; Terry et al., 2000b; Ravna and Terry, 2004; Walsh and Hacker, 2004; Root et al., 2005; Hacker, 2006; Carswell et al., 2006; Young et al., 2007; Butler et al., 2013). Root et al. (2005) used the spatial distribution of eclogites and K-white mica $^{40}Ar/^{39}Ar$ ages to conclude that the UHP rocks crop out in three east–southeast-plunging antiforms: the southern (Nordfjord), central (Sørøyane), and northern (Nordøyane) UHP domains (Fig. 1a).

There is an overall northwestward increasing gradient in the peak *P–T* conditions recorded across the WGR (e.g., Krogh, 1977; Lappin and Smith, 1978; Griffin et al., 1985; Cuthbert et al., 2000; Labrousse et al., 2004; Hacker et al., 2010). The southern UHP domain contains a transition from HP quartz eclogite (2.4 GPa and 600 ºC) to UHP coesite and microdiamond eclogite (> 3.5 GPa and 750 ºC; Cuthbert et al., 2000; Young et al., 2007; Smith and Goddard, 2013). The central UHP domain records *P-T* conditions up to 3.2 GPa and 795 ºC (Krogh Ravna in Carswell et al., 2003b; Root et al., 2005). Peak *P-T* conditions reached a maximum of 3.8–3.9 GPa and 820–850 ºC for eclogites and microdiamond-bearing paragneiss within the northern UHP domain (Terry et al., 2000b; Carswell et al., 2006). Even greater *P–T* estimates have been suggested for peridotite within the host gneiss of the northern WGR (e.g., Vrijmoed et al., 2006, 2008; Scambelluri, et al., 2008; Spengler et al., 2009; van Roermund, 2009).

2.2 Geochronological overview of WGR Scandian UHP metamorphism

Over the past ~35 years, many studies of the WGR have focused on the timing of peak UHP metamorphism during the subduction of Baltica–Avalonia beneath Laurentia during the Scandian orogeny. These studies and the techniques used to resolve the timing and duration of the UHP event are summarized below and in Table 1. Reported uncertainties are at the 2-sigma or 95% confidence level unless otherwise stated.

2.2.1 Sm-Nd geochronology

The first Sm-Nd eclogite ages ever obtained were garnet–omphacite isochron dates from the WGR (Griffin and Brueckner, 1980, 1985); they yielded an average age of ca. 425 Ma, discrediting initial suggestions of a Precambrian age for the eclogite-facies metamorphism (e.g., Krogh, 1977). Additional Sm-Nd studies of eclogites throughout the WGR gave younger isochron dates of ca. 412–408 Ma (Mearns, 1986; Mørk and Mearns, 1986; Jamtveit et al., 1991; Carswell et al., 2003b; see section 2.3). Peridotites within the northern UHP domain yielded Sm-Nd garnet–omphacite isochron dates interpreted to represent prograde subduction at 429.5 ± 3.1 Ma (Spengler et al., 2009) and cooling at 393.4 ± 3.4 Ma and 380.7 ± 5.7 Ma (Vrijmoed et al., 2006). More recent studies that combined the Lu-Hf and Sm-Nd isotopic systems for HP eclogites across the WGR show a ~20 Myr range of prograde garnet growth during eclogite-facies metamorphism from ca. 419–410 Ma (Lu-Hf) and ca. 414–397 Ma (Sm-Nd) (Kylander-Clark et al., 2007, 2009).

2.2.2 Rb-Sr geochronology

Isochron dates using the Rb-Sr system have also been described from southern WGR eclogites. Griffin and Brueckner (1985) reported an Rb-Sr isochron date of 397 ± 8 Ma (2%) (recalculated by Root et al., 2004) using whole-rock and mineral fractions of the Verpeneset eclogite in the southern UHP domain. Three eclogites collected ~65 km south of the southern UHP domain yielded a weighted-mean multi-mineral Rb-Sr isochron date of 404.0 ± 2.1 Ma (Glodny et al., 2008).

2.2.3 U-Th-Pb monazite

Terry et al. (2000b) employed secondary ion mass spectrometry (SIMS) and electron-microprobe (EMP) techniques on a microdiamond-bearing gneiss to constrain UHP metamorphism in the northern UHP domain using U-Th-Pb monazite geochronology. Monazite inclusions within inferred UHP garnet of the microdiamond sample yielded a SIMS weighted-mean $^{206}Pb/^{238}U$ age of 415.0 ± 6.8 Ma. The first LASS study of monazite obtained four weighted-mean $^{206}Pb/^{238}U$ ages of 426.5 ± 5.6 Ma, 408.8 ± 6.3 Ma, 395.0 ± 3.9 Ma, and 390.3 ± 4.9 Ma from a HP garnet–muscovite–kyanite gneiss from Leinøya in the central UHP domain (Kylander-Clark et al., 2013). Based on the variation in MREE–HREE patterns, Sr abundances, and Eu anomalies, Kylander-Clark et al. (2013) interpreted monazite (re)crystallization to have occurred at ca. 427–395 Ma in the presence of garnet, and the breakdown and recrystallization of plagioclase to have occurred between ca. 427 Ma and 390 Ma.

2.2.4 U-Th-Pb zircon

Much effort has focused on U-Pb zircon multi- and (sparse) single-grain ID-TIMS studies of WGR (U)HP eclogite. The northern WGR at Averøya hosts a probable UHP eclogite with the oldest zircon age of 415.2 ± 0.6 Ma (multi-grain weighted-mean ^{206}Pb/^{238}U age), whereas younger single zircon grains, interpreted to date an amphibolite-facies overprint, gave ^{206}Pb/^{238}U ages of 410.8 ± 1.4 Ma and 409.6 ± 1.5 Ma (Krogh et al., 2011). Furthermore, within the northern UHP domain, multi-grain zircon fractions from the eclogitized margin of the Flem Gabbro yielded a weighted-mean ^{206}Pb/^{238}U age of 409 ± 3 Ma, and a probable UHP eclogite from Midsund Bruk yielded a ^{206}Pb/^{238}U age of 405 ± 1 Ma (Krogh et al., 2011). Lastly, a HP hornblende eclogite from Lepsøya gave a weighted-mean, multi-grain ^{206}Pb/^{238}U age of 412 ± 1 Ma (Krogh et al., 2011).

The same zircon separates from the ca. 405 Ma Midsund Bruk eclogite described above were analyzed by LASS, which produced weighted-mean 207-corrected ^{206}Pb/^{238}U ages of 420.6 ± 8.4 Ma and 400.4 ± 8.0 Ma and a range of dates from ca. 409–407 Ma (Kylander-Clark et al., 2013). The three age populations are distinguished by different REE patterns (e.g., variation in MREE and a lack of a steep, positive HREE pattern and negative Eu anomalies) and are interpreted to record protracted (re)crystallization at eclogite-facies conditions (Kylander-Clark et al., 2013).

An early multi-grain ID-TIMS study of the Ulsteinvik eclogite within the central UHP domain (Fig. 1b) gave an initial age of 401± 20 Ma, marking the first record of a Devonian history for the WGR (Krogh et al., 1974). Subsequent analyses of zircon multi-grain fractions from the Ulsteinvik eclogite provided a more-precise weighted-mean ^{207}Pb/^{206}Pb age of 401.6 ± 1.6 Ma (Tucker et al., 2004). Some of these zircons contain omphacite or rutile, and coesite inclusions were discovered in the zircon separates after the TIMS work (Carswell et al., 2003a), leading these authors to interpret the 401.6 ± 1.6 Ma age as the best record of UHP metamorphism within the WGR.

The first study to combine chemical-abrasion ID-TIMS (CA-TIMS, Mattinson, 2005), high-spatial resolution SIMS, and trace-element analysis of zircon washes by solution ICP-MS was completed in the WGR by Root et al. (2004). Multi-grain zircons analyses on the Flatraket eclogite yielded discordant U-Pb dates interpreted to represent zircon (re)crystallization at ca. 405–400 Ma with minor discordance attributed to inherited cores. Eclogite-facies garnet inclusions in the zircons and flat HREE zircon profiles revealed from the TIMS wash solutions are compatible with (re)crystallization at or near peak metamorphism. Zircons from the eclogites at Verpeneset and Langenes also yielded discordant CA-TIMS data compatible with ca. 400 Ma metamorphic zircon and 1.6 Ga igneous zircon (Root et al., 2004). Finally, at Hjelmelandsdalen near the southern UHP domain, two air-abraded single grains from a (U)HP eclogite gave an ID-TIMS weighted-mean $^{206}Pb/^{238}U$ age of 405 ± 2 Ma (Young et al., 2007).

2.3 UHP eclogites of the central and southern domains

In this study, two UHP eclogites, Ulsteinvik and Saltaneset, were collected from the central and southern WGR, respectively (Fig. 1a). These sample localities have been extensively studied and are known to preserve or are interpreted to have once contained coesite (Cuthbert et al., 2000; Wain et al., 2000; Carswell et al., 2003a, 2003b). The large Ulsteinvik eclogite of the central UHP domain is exposed on Hareidlandet and extends to the nearby islands of Dimnøya and Hatløy (Fig. 1b). This internally layered eclogite is one of the largest eclogite bodies within the WGR (~6 km long by 0.2–1.5 km wide) and is hosted in predominantly garnet–biotite–kyanite gneiss (Mysen and Heier, 1972). The quartz-bearing eclogite contains accessory rutile and minor kyanite and amphibole. The eclogite is pervasively retrogressed with omphacite replaced by multiple stages of symplectite with progressively less sodic-clinopyroxene and more-calcic plagioclase (Mysen, 1972; Mysen and Heier, 1972). Further evidence of retrogression includes partial replacement of garnet by hornblende and biotite with plagioclase (Carswell et al., 2003a). As described above, zircons with inclusions of omphacite, garnet, rutile, quartz, and coesite have been identified from the Ulsteinvik eclogite (Krogh et al., 1974; Carswell et al., 2003a). ID-TIMS dating provided a weighted-mean $^{207}Pb/^{206}Pb$ age of 401.6 ± 1.6 Ma (n = 4, MSWD = 0.48); scatter in the isotopic dates was inferred to be a result of recent Pb loss (Tucker et al., 2004).

The coesite-bearing Saltaneset eclogite, first reported in detail by Wain et al. (2000), is located ~2 km south of Selje within the southern UHP domain (Fig. 1c). The main Saltaneset eclogite is a tabular, compositionally layered body (20 m long by ~3–5 m wide), consisting of mostly omphacite-rich layers and fewer garnet-rich, quartz layers that are 3–25 mm thick (Carswell et al., 2003b; Renedo et al., 2014). The eclogite is within a mylonite zone of fine-grained, quartzofeldspathic gneiss (Renedo et al., 2014). Relict coesite and polycrystalline quartz are preserved within garnet from a quartz layer of the Saltaneset eclogite (Cuthbert et al., 2000; Wain et al., 2000). Carswell et al. (2003b) described two generations of garnet within a garnet-rich quartz layer and argued that the layers were originally garnet-bearing coesitites based on the presence of abundant quartz pseudomorphs after coesite within the second generation of garnet. An Sm-Nd isochron age (garnet–omphacite–whole rock) of 408.3 ± 6.7 Ma (MSWD = 0.81) was determined for this Saltaneset eclogite (Carswell et al., 2003b).

3. Methods

Representative samples of the Ulsteinvik eclogite and the garnet–quartz- and omphacite-rich layers of the Saltaneset eclogite were collected. Zircon was extracted from the whole-rock

Ulsteinvik sample, whereas individual garnet–quartz and omphacite-rich layers from the Saltaneset eclogite were separated and then separately crushed to extract zircon from each layer. Polished grain mounts were prepared and imaged by cathodoluminescence (CL) to reveal zoning (Fig. 2). This study utilized two separate geochronologic techniques on the same zircons: 1) high-spatial resolution laser ablation split-stream (LASS)–inductively coupled plasma–mass spectrometry, allowing for the simultaneous collection of U-Th-Pb data and trace element data for individual spot analysis (Kylander-Clark et al., 2013); and 2) high-precision, single-grain U-Pb chemical abrasion ID-TIMS and trace element analysis (TIMS-TEA; Mattinson, 2005; Schoene et al., 2010). Chemical abrasion removes high-U zones of the zircon susceptible to Pb loss, therefore minimizing or wholly eliminating Pb-loss correction (Mattinson, 2005). TIMS-TEA allows for the same zircon dated by U-Pb ID-TIMS to be analyzed for trace element composition by solution ICP-MS (Root et al., 2004; Schoene et al., 2010).

Transects across different generations of garnet within the Ulsteinvik and Saltaneset eclogites were analyzed by LA-ICP-MS in thin sections of the same rocks that were crushed (Fig. 6). Trace-element data from both zircon and garnet are normalized to the chondrite values of Sun and McDonough (1989).

LASS analyses were first performed to identify Scandian zircon. From there, Scandian whole grains or Scandian subdomains *within* grains were targeted for ID-TIMS analysis. A combination of single grains, fragments of grains, and multiple fragments from the same grain were analyzed by ID-TIMS to try to identify grain-to-grain and intragrain heterogeneity that might cause inaccurate and/or mixed ages (e.g., Mundil et al., 2001; Schoene, 2013). All grains were annealed at 900 ºC for 60 hours and chemically abraded at 220 ºC for 12 hours (Mattinson et al., 2005). ID-TIMS analyses have typical uncertainties of ~0.05% for Th-corrected $^{206}Pb/^{238}U$

weighted-mean dates and <0.2% for individual Th-corrected $^{206}Pb/^{238}U$ dates that are inversely proportional to the radiogenic/common Pb ratio (Pb*/Pbc; Table 3). Most ID-TIMS analyses do not define a single population and are reported as individual Th-corrected $^{206}Pb/^{238}U$ dates. In comparison, LASS $^{206}Pb/^{238}U$ dates have typical uncertainties of ~1–2% for single spot analyses, including both analytical and propagated uncertainties (Table 2). Reported uncertainties throughout the text, data tables, and figures are at the 2-sigma or 95% confidence level unless otherwise stated.

We first report zircon U-Pb and trace element data from grains that were analyzed by both LASS and TIMS-TEA. These results are then compared to zircons analyzed by LASS only. Finally, zircon-garnet trace element partition coefficients are calculated to link U-Pb dates to the *P-T* history of the samples (Figs. 4a–b, 5, 6, and 7). All LASS and ID-TIMS inherited zircon analyses are presented on concordia diagrams in Fig. S1. The online supporting information provides a more-detailed description of the methodology for U-Pb LASS and TIMS-TEA zircon analyses and data tables for the zircon and garnet trace-element analyses (Tables 4 and 5, respectively).

4. Results

4.1 U-Pb zircon LASS and ID-TIMS geochronology

Zircons extracted from the Ulsteinvik eclogite within the central UHP domain are mostly irregular to sub-rounded, and CL images reveal patchy- and polygonal-sector zoning (Fig. 2). In comparison, zircons from the garnet–quartz and omphacite layers of the Saltaneset eclogite from the southern UHP domain are rounded to sub-rounded and have patchy zoning and homogenous, dark-CL rim overgrowths (Fig. 2). No difference in the CL patterns of the zircons from the two layers was detected. All zircons are interpreted to be metamorphic based on morphology, zoning (e.g., Corfu et al., 2003), and low (< 0.04) Th/U ratios (Fig. S2a; Tables 2 and 3). LASS zircon analyses targeted both the cores and rims of grains (Fig. 2; Table 2).

4.1.1 Ulsteinvik eclogite

Eclogite sample 8815E was collected from the layered body on the island of Hareidlandet, approximately 1 km southeast of Ulsteinvik (Fig. 1b). Analysis of thirteen zircons by LASS yields single-spot $^{206}Pb/^{238}U$ dates ranging from 412.8 ± 5.4 Ma to 400.5 ± 4.7 Ma (n = 24; Figs. 3b and 4a; Table 2). ID-TIMS results from thirteen whole grains or microsampled fragments of the same zircons give Th-corrected $^{206}Pb/^{238}U$ dates from 409.6 ± 0.6 Ma to 401.3 ± 0.4 Ma (n = 15; Figs. 3a and 4a; Table 3). To test for dispersion of ID-TIMS dates within a single grain, a ~200 μm zircon was microsampled, and the three fractions yield indistinguishable $^{206}Pb/^{238}U$ dates of 401.9 ± 0.2 Ma, 401.9 ± 0.4 Ma, and 402.1 ± 0.3 Ma (z1 in Figs. 4a and 2; Table 3). Overall, the ID-TIMS results cluster into two populations, ca. 409–407 Ma and ca. 402 Ma, but only the youngest population yielded a weighted-mean $^{206}Pb/^{238}U$ date with a statistically acceptable MSWD (401.9 ± 0.1 Ma, MSWD = 1.9, n = 5) (Fig. 4a). Ten additional zircons analyzed by LASS alone yielded $^{206}Pb/^{238}U$ dates ranging from 412.0 ± 5.3 Ma to 397.2 ± 5.2 (n = 10; Fig. 4a; Table 2) and older dates of ca. 475–430 Ma (n = 5; Fig. 3b; Table 2).

4.1.2 Saltaneset eclogite: garnet–quartz and omphacite layers

Sample NW13-02 was collected from an eclogite within the 60 m Saltaneset mylonite shear zone (Fig. 1c) (Renedo et al., 2014). Zircon LASS analyses from four zircons extracted from the garnet–quartz layer give $^{206}Pb/^{238}U$ dates of 407.8 ± 5.1 Ma to 398.1 ± 8.7 Ma (n = 4; Figs. 3b and 4b; Table 2). These same zircons yielded ID-TIMS $^{206}Pb/^{238}U$ dates ranging from 409.0 ± 0.4 Ma to 401.4 ± 0.2 Ma (Figs. 3a and 4b; Table 3). These results reveal two populations with weighted-mean $^{206}Pb/^{238}U$ dates of 408.8 ± 0.2 Ma (n = 2) and 401.4 ± 0.1 Ma (n = 2), respectively (Fig. 4b). Nine additional zircons analyzed by ID-TIMS yield discordant dates, which when combined with the Scandian ID-TIMS dates reveal weak discordia arrays with upper-intercept ages of ca. 1560 Ma and ca. 943 Ma (Fig. S1; Table 3). The remaining zircons analyzed by LASS produced Scandian $^{206}Pb/^{238}U$ dates from 413.4 ± 9.8 Ma to 396.8 ± 8.8 Ma (n= 10; Figs. 3b and 4b; Table 2). Similar to the ID-TIMS results, LASS results also include discordant analyses that define a discordia array with an upper-intercept of ca. 970 Ma (Fig. S1; Table 2); however, LASS analyses do not reproduce the older ca. 1600 Ma discordia array revealed by ID-TIMS analyses.

Only one zircon from the omphacite-rich layer (NW13-02-O) yielded a Scandian age for both techniques. LASS analysis resulted in a $^{206}Pb/^{238}U$ date of 404.1 ± 5.1 Ma, and ID-TIMS analysis yielded a $^{206}Pb/^{238}U$ date of 396.7 ± 1.4 Ma (Figs. 2, 3a, and 4b; Tables 2 and 3, respectively). Other zircons from NW13-02-O yielded older, discordant ID-TIMS dates defining a discordia array, suggesting a protolith age of ca. 936 Ma (Fig. S1; Table 2). Additional zircons dated by LASS yielded $^{206}Pb/^{238}U$ dates ranging from 414.4 ± 5.8 Ma to 398.4 ± 8.1 Ma (n = 5; Figs. 3b and 4b; Table 2), as well as two discordia arrays with upper intercepts of ca. 1599 Ma and 954 Ma (Fig. S1).

4.2 Zircon trace-element data

LASS trace element results are shown for the Ulsteinvik eclogite and the Saltaneset garnet–quartz and omphacite layers in Figs. 5a–c. The solution ICP-MS trace element data obtained from the ID-TIMS washes are in Figs. 5d–e, S2a–b, and Table 4. All Scandian solution ICP-MS analyses for the Saltaneset garnet–quartz and omphacite layers are combined in Fig. 5e as there is only a single Scandian zircon ID-TIMS date from the omphacite layer.

4.2.1 Ulsteinvik eclogite LASS and solution ICP-MS zircon trace element data

The LASS zircon REE patterns from the Ulsteinvik eclogite reveal two distinct patterns. Scandian (ca. 413–397 Ma) zircons analyzed by LASS record a flat HREE slope (Lu_N/Gd_N = 0.62–4.40; n = 34) and mostly flat-to-positive Eu anomalies ($Eu/Eu^* = Eu_N/(Sm_N \times Gd_N)^{0.5}$ = 0.75–1.93; n = 29), although slightly negative Eu anomalies were also obtained (Eu/Eu* = 0.56–0.73; n = 5) (Fig. 5a; Table 4). The individual REE patterns of most analyses reveal an overall higher concentration of MREE and HREE for the younger Scandian analyses (ca. 405–397 Ma) compared to the older Scandian analyses (ca. 413–406) (Fig. 5a; Table 4). The second pattern represented by inherited dates (ca. 475–430 Ma; n = 5) is characterized by an increase in the overall REE concentration, steep HREE slopes (Lu_N/Gd_N = 42–128), and prominent-to-flat Eu anomalies (Eu/Eu* = 0.35–0.94) (Fig. 5a; Table 4).

The solution ICP-MS trace element patterns of Scandian (ca. 409–402 Ma) Ulsteinvik zircons are similar to laser ablation analyses of the same zircons: flat HREE slopes (Lu_N/Gd_N = 0.54–5.51, n = 14) and a lack of strongly-negative Eu anomalies (Eu/Eu* = 0.88–1.53, n = 14) (Figs. 5d and S2a). These analyses record an overall greater abundance of MREE–HREE for the younger analyses in comparison to the laser-ablation analyses; however, similar to the LASS analyses, there is a correlation between younger Scandian dates and higher MREE–HREE abundances (Figs. 5d and S2b; Table 4). Furthermore, the younger Scandian ca. 402 Ma zircons yielded greater Y/Sc and Zr/Hf ratios (Fig. S2b).

4.2.2 Saltaneset garnet–quartz and omphacite layers zircon LASS and solution ICP-MS trace element data

Zircon LASS trace element data from the garnet–quartz layer, NW13-02-G, also reveal two separate REE patterns. The Scandian (ca. 413–397 Ma) zircons are characterized by flat (Lu_N/Gd_N = 1.87–3.93, n = 12) to slightly positive (Lu_N/Gd_N = 5.81–10.38, n = 2) HREE slopes and absent (0.75–1.24, n = 7) to slightly negative Eu anomalies (Eu/Eu* = 0.43–0.64, n = 7) (Fig. 5b; Table 4). In comparison, inherited (ca. 966–528 Ma) zircons show more enriched REE patterns, with steep HREE slopes (Lu_N/Gd_N = 7.95–97.87, n = 39) and prominently negative (Eu/Eu* = 0.19–0.48, n = 35) to slightly negative Eu anomalies (Eu/Eu* = 0.57–0.70, n = 3) (Fig. 5b; Table 4).

The omphacite-rich layer, NW13-02-O, yielded LASS zircon REE patterns similar to the Saltaneset garnet–quartz layer and the Ulsteinvik eclogite. The youngest population of zircons (ca. 414–398 Ma) is represented by flat (Lu_N/Gd_N = 1.95–3.24, n = 3) to slightly-positive HREE slopes (Lu_N/Gd_N = 5.33–8.89, n = 3). These grains lack negative Eu anomalies (Eu/Eu*=0.80–1.47, n = 5), with the exception of a single analysis (Eu/Eu*=0.70) (Fig. 5c, Table 4). In contrast, ca. 1600–433 Ma zircons are distinguished by enrichment in all REE, especially HREE. These inherited grains have steep HREE slopes (Lu_N/Gd_N = 4.34–150.7, n = 39). A variety of Eu anomalies are preserved, from strongly negative to absent (Eu/Eu* = 0.23–0.83, n = 40) (Fig. 5c; Table 4).

Individual Scandian zircon solution ICP-MS REE patterns for the Saltaneset garnet–quartz layer (ca. 409–402 Ma) and a single analysis from the omphacite layer (ca. 397 Ma) have positive Eu anomalies (Eu/Eu* = 0.75–1.05, n = 5) and are depleted in HREE, producing HREE slopes similar to Scandian LASS analyses for both layers. The depleted HREE signatures show flat to slightly positive slopes (Lu_N/Gd_N = 1.72–3.34, n = 5) (Figs. 5e and S2a–b; Table 4). Similar to the Ulsteinvik solution ICP-MS analyses, the ca. 402 Ma grains from the Saltaneset garnet–quartz layer have increased MREE–HREE abundances and greater Y/Sc and Zr/Hf ratios (Fig. S2b). Solution ICP-MS analyses (ca. 1512–425 Ma) for the inherited grains are similar to the LASS REE patterns of inherited zircons from both Saltaneset eclogite layers (Fig. 5e). The individual zircon trace-element profiles show pronounced to slightly-negative Eu anomalies (Eu/Eu* = 0.34–0.72, n = 5) and strong enrichment in HREE with steep slopes (Lu_N/Gd_N = 5.29–46.47, n = 5) (Fig. 5e; Table 4).

4.3 Garnet LA-ICP-MS trace element data

4.3.1 Ulsteinvik eclogite garnet LA-ICP-MS trace-element data

Garnet within the Ulsteinvik eclogite consists of large (1–4 mm), fractured porphyroblasts and later polycrystalline garnet in the matrix and rimming some of the early porphyroblasts. Transects across the porphyroblasts and the polycrystalline matrix garnet from the same portion of the eclogite in which zircon was extracted revealed variable trace-element signatures. The porphyroblasts have slight variation in LREE composition and flat MREE–HREE signatures (Lu_N/Gd_N = 0.69–1.43, n = 141) (Fig. 6a; Table 5). In contrast, late polycrystalline garnet in the matrix and rimming early garnet have lower and more variable LREE, with more consistent MREE and HREE (Lu_N/Gd_N = 0.77–3.74, n = 39) (Fig. 6b; Table 5). Both generations of garnet preserve flat Eu anomalies (Eu/Eu* = 1.10–1.67, n = 198) (Figs. 6a–b; Table 5).

4.3.2 Saltaneset garnet–quartz and omphacite layers garnet LASS trace element data

The Saltaneset eclogite contains garnet within both of its layers. The large (1–3 mm), subhedral garnets located within the quartz vein have similar LREE, whereas core-to-rim variation in MREE and HREE is preserved. The rims show flat patterns (Lu_N/Gd_N = 2.21–4.79, n = 8) that transition to negative HREE slopes for the garnet core (Lu_N/Gd_N = 0.15–0.96, n = 17) (Fig. 6d; Table 5). In comparison, small (0.5–0.8 mm) anhedral garnets from the omphacite-rich layer have homogenous trace element profiles with slightly-positive HREE slopes (Lu_N/Gd_N = 2.25–5.72, n = 11) (Fig. 6c; Table 5). Garnet analyses within both layers of the eclogite have positive Eu anomalies (Eu/Eu* = 0.73–1.20, n = 36) (Figs. 6c–d; Table 5).

4.3.3 Zircon-garnet trace-element partition coefficients

Rare earth element partitioning between zircon and garnet (i.e., D_{REE} (zrn/grt)) was calculated for the Ulsteinvik and Saltaneset eclogite layers to further assess whether zircon (re)crystallized in equilibrium with garnet (Fig. 7). To determine D_{REE} (zrn/grt), average trace element compositions for the two zircon populations (ca. 409–407 Ma and ca. 402 Ma) from each sample were paired with the average composition of different garnet populations (see below). For consistency, both solution ICP-MS (Fig. 7) and laser ablation ICP-MS (Fig. S3) trace-element analyses are used separately in the partition coefficient calculations. However, the trends in REE (Lu_N/Gd_N and MREE–HREE abundances) versus age from both techniques are similar and thus the calculated distribution coefficients are similar (Figs. 5 and S2a–b). As some LREE were below detection limits for most of the zircon solution ICP-MS analyses, D_{LREE} values were only calculated from a few analyses.

Within the Ulsteinvik eclogite, there are two garnet populations: 1) early garnet porphyroblasts; and 2) late, recrystallized garnet as a matrix phase and as rims on the porphyroblasts. The trace element data for the porphyroblasts show consistent LREE–HREE patterns, whereas the later recrystallized garnet have more variably-depleted LREE (Figs. 6a–b; Table 5). The overlap of some LREE–MREE analyses for the two garnet types may reflect growth of early and late garnet under similar P-T conditions (Fig. 6b). D_{REE} was calculated from pairing the older zircon population with the early garnet porphyroblasts and the younger zircon population with the late-recrystallized garnet (Fig. 7). The young (ca. 402 Ma) zircons/late garnets have D_{REE} near unity for the MREE–HREE (Fig. 7). A similar, flat D_{HREE} partitioning pattern is observed for the old (ca. 409 Ma) zircons/early garnets; however, the values are slightly less than unity (Fig. 7). In addition, the D_{MREE} values decrease with decreasing atomic number for the old zircon/early-garnet pairs (Fig. 7).

For the Saltaneset eclogite, the garnet cores from the quartz layer have greater MREE (Sm–Tb) and less HREE (Tm–Lu) relative to their rims (Fig. 6d; Table 5). D_{REE} for the garnet–quartz layer were calculated by pairing the trace element compositions of the older zircon population with the garnet cores, and the younger zircon population with the garnet rims (Fig. 7). D_{HREE} and D_{MREE} for the young zircon/garnet rim compositions are consistent and greater than unity, whereas the older zircon/garnet core pairs indicate preferential partitioning of the Lu into zircon ($D_{Lu} = 5.81$), with D_{REE} decreasing to near-unity values at Dy and for the remaining MREE (Fig. 7).

In comparison to the garnet–quartz layer, garnets from the Saltaneset omphacite-rich layer have consistent core-to-rim trace element profiles, with weakly positive HREE slopes (Fig. 6c; Table 5). D_{REE} for the Saltaneset omphacite layer were calculated with the zircon trace element composition of the single ID-TIMS analysis and the LA-ICP-MS average trace element composition of the homogeneous garnet; these results show consistent D_{REE} values slightly above unity from Lu–Sm (Fig. 7).

5. Discussion

The preservation of (U)HP eclogites and mantle peridotites across 30,000 km^2 of the WGR provides irrefutable evidence for the deep subduction and exhumation of a large body of continental crust during the late stages of the Caledonian orogeny. Previous geochronological investigations have concluded that the rocks remained at eclogite-facies depths from ca. 425–400 Ma. In order for the subducted material to have remained at eclogite-facies conditions for > 20 Myr prior to exhumation, studies have argued that either multiple UHP events occurred at different times across the WGR or that the subducted crust was thick and subduction was slow (Root et al., 2005; Hacker, 2007; Kylander-Clark et al., 2009). Evaluating these endmember models requires constraining the timing and duration of UHP metamorphism at different locations across the WGR.

5.1 Zircon: Ulsteinvik and Saltaneset eclogites

LASS and solution ICP-MS analyses from all of the Scandian zircons from both the Ulsteinvik and Saltaneset eclogites show REE patterns consistent with (re)crystallization during eclogite-facies metamorphism, with depleted, flat HREE signatures and weak, negative Eu anomalies (Figs. 5 and S2a). The LASS U-Pb zircon results from the Ulsteinvik eclogite presented in this study reveal protracted Scandian zircon (re)crystallization at eclogite-facies conditions from ca. 413–397 Ma, with single-crystal ID-TIMS analyses suggesting two zircon (re)crystallization events at ca. 409–407 Ma and 401.9 ± 0.1 Ma (Figs. 3a and 4a). Previous studies of the

Ulsteinvik eclogite had documented UHP eclogite-facies inclusions within zircon (i.e., omphacite, garnet, rutile, quartz, and coesite) and argued that the 401.6 ± 1.6 Ma zircon age best represents the timing of WGR UHP metamorphism (Krogh et al., 1974; Carswell et al., 2003a). However, this Ulsteinvik zircon age is a multi-grain, weighted-mean $^{207}Pb/^{206}Pb$ age derived from four different U-Pb ratios; thus, this age may incorporate and average multiple generations of zircon (re)crystallization. The younger of the two populations revealed by ID-TIMS is equivalent to the earlier reported value of 401.6 ± 1.6 Ma; however, the older population reveals an earlier eclogite-facies history than previously reported, suggesting that the Ulsteinvik body was at (U)HP conditions by at least ca. 409 Ma.

The layered Saltaneset eclogite previously yielded an Sm-Nd garnet–omphacite–whole rock isochron date of 408.3 ± 6.7 Ma (n = 3, MSWD = 0.81) (Carswell et al., 2003b). In comparison to the Sm-Nd age, U-Pb zircon results from the Saltaneset eclogite garnet–quartz layer suggest a prolonged (U)HP history, with LASS analyses yielding a range of Scandian dates from ca. 413–397 Ma and ID-TIMS results revealing a bimodal population of 408.8 ± 0.2 Ma and 401.4 ± 0.1 Ma (Figs. 3a and 4b; Tables 2 and 3). As only two zircons make up the ca. 409 Ma ID-TIMS population, it is possible that this population represents mixing of minor inherited zircon domains with the ca. 402 Ma age domains (Fig. S1); however, the calculated discordia arrays show scatter (high MSWDs), the ca. 409 Ma dates overlap concordia within uncertainty (Fig. 3a), and the previously reported Sm-Nd isochron age is in good agreement with this U-Pb age. Furthermore, the solution trace element data shows distinct MREE–HREE abundances and steepness of the HREE patterns for the inherited, ca. 409 Ma, and ca. 402 Ma zircon populations (Figs. 5a–e and S2b). Therefore, the ca. 409 Ma zircons in the Saltaneset garnet-quartz layer likely record an eclogite-facies event that is also evident in the Ulsteinvik eclogite.

Only a single Scandian zircon was dated by both techniques from the omphacite-rich layer, as the majority of the grains were inherited (Figs. 3b and S1; Tables 2 and 3). This Scandian zircon revealed the youngest ID-TIMS date of this study: 396.7 ± 1.4 Ma (Fig. 4b; Table 3). LASS analyses from this layer reveal a range of Scandian dates from ca. 414–398 Ma and a similar inherited zircon population as recorded in the quartz-dominated layer (Figs. 4b and S1; Table 2). Based on these similar zircon inheritance patterns, it is likely that the Saltaneset omphacite and garnet–quartz layers underwent the same P–T history.

5.2 Zircon-garnet equilibrium patterns

Multiple studies have used trace element partitioning between zircon and garnet as a means of assessing equilibrium between the two minerals across a range of temperatures in granulite-facies rocks (e.g., Harley et al., 2001; Rubatto, 2002; Hermann and Rubatto, 2003; Rubatto and Hermann, 2003; Hokada and Harley, 2004, Kelly and Harley, 2005; Buick et al., 2006; Rubatto et al., 2006; Harley and Kelly, 2007) and to a lesser extent in eclogite-facies rocks (Fig. 7; e.g., Rubatto, 2002; Rubatto and Hermann, 2003; Baldwin et al., 2004; Monteleone et al., 2007; Rubatto and Hermann, 2007b).

The calculated zircon–garnet partition coefficients for the Ulsteinvik eclogite and Saltaneset eclogite layers show two different D_{HREE} patterns (Fig. 7). The first is represented by constant D_{REE} values, as observed for the Ulsteinvik eclogite, the Saltaneset garnet–quartz young zircon/rim garnet pairs, and the Saltaneset omphacite-layer (Fig. 7). The second, from the old zircon/garnet core compositions from the Saltaneset garnet–quartz layer, is marked by a decrease in HREE partitioning into zircon from Lu to Dy (Fig. 7).

Both D_{HREE} patterns described above for the Ulsteinvik and Saltaneset eclogites have previously been suggested to be indicative of zircon/garnet equilibrium. The flat pattern with near-unity D_{HREE} values has been observed in natural eclogite- and granulite-facies rocks and in experiments (e.g., Harley et al., 2001; Whitehouse and Platt, 2003; Hokada and Harley, 2004; Kelly and Harley, 2005; Harley and Kelly, 2007; Monteleone et al., 2007; Taylor et al., 2014). The second pattern, marked by a decrease in zircon partitioning from HREE–MREE, has been inferred to represent equilibrium between zircon and garnet in eclogites and experimental studies (e.g., Baldwin et al., 2004; Rubatto, 2002; Rubatto and Hermann, 2003, 2007b). In contrast to the zircon/garnet pairings discussed above, if the different garnet and zircon REE compositions are switched (i.e., young/core and old/rim), similar D_{REE} patterns are obtained. Based on these results, it is suggested that the different zircon and garnet populations from both eclogites were likely in equilibrium during this prolonged period of eclogite-facies metamorphism; thus, (re)crystallization of zircon under garnet-stable conditions likely occurred from ca. 409–402 Ma.

5.3 Older (≥430 Ma) Caledonian Eclogite Ages

In addition to the Scandian dates, zircons from the Ulsteinvik eclogite also reveal a nearly continuous spread of older concordant Caledonian dates that range from ca. 475–430 Ma (Fig. 3b; Table 2). Root et al. (2005) suggested that the Ulsteinvik eclogite is allochthonous based on the similarity of the host rock lithologies, including garnet–biotite–kyanite schist, quartzite, marble (Mysen and Heier, 1972), and coarse augen gneiss, to the allochthonous Blåhø and Risberget Nappes, exposed to the north (Robinson, 1995). Furthermore, the ca. 475–430 Ma zircons overlap with ca. 459 Ma eclogite zircon ages, interpreted to be mainly igneous (Th/U = 0.19–0.72), from the Blåhø Nappe exposed ~150 km to the east and ca. 440 Ma eclogite metamorphic zircon (re)crystallization ages (Th/U = 0.03–0.13) from allochthons exposed ~60 km to the southeast (Walsh et al., 2007). The metamorphic (re)crystallization ages are possibly related to allochthon emplacement (e.g., Hacker and Gans, 2005).

In comparison, the Saltaneset layered eclogite records evidence of the Gothian and Sveconorwegian orogenic events (e.g., Skår, 2000; Austrheim et al., 2003), with upper intercept ages of ca. 1600–1560 Ma and ca. 970–936 Ma from two separate discordia arrays (Fig. S1). These results suggest the metabasite protolith likely intruded the WGC basement rocks and crystallized at ca. 1600 Ma. It was then reworked during the Sveconorwegian and Caledonian orogenies. Similar eclogite protolith ages have been obtained across the WGR for both events (e.g., Root et al., 2004; Walsh et al., 2007) in addition to the abundant record of these events recorded by felsic basement rocks (e.g., Brueckner, 1972, 1979; Carswell and Harvey, 1985; Tucker et al., 1990, 2004; Skår et al., 1994; Skår, 2000; Austrheim et al., 2003; Skår and Pederson, 2003; Røhr et al., 2004, 2013; Root et al., 2005; Glodny et al., 2008; Kylander-Clark et al., 2008; Krogh et al., 2011; Corfu et al., 2013).

5.4 UHP metamorphism in the central and southern UHP domains

New LASS and ID-TIMS results support previous conclusions that UHP metamorphism occurred from ca. 410–400 Ma in the central and southern UHP domains (Krogh et al., 1974; Mearns, 1986; Carswell et al., 2003a, 2003b; Root et al., 2004; Tucker et al., 2004; Young et al., 2007). However, the new high-precision, single-crystal data also indicate that zircon (re)crystallization was locally episodic, at ca. 409–407 Ma and at ca. 402 Ma, rather than continuous. The possibility of prolonged subduction has been inferred on a larger scale from U-Pb zircon, Lu-Hf garnet, and Sm-Nd garnet dates (Kylander-Clark et al., 2007, 2009; Krogh et al., 2011). This is the first study, however, to record multiple discrete ages of (U)HP zircon (re)crystallization events within individual samples from two separate localities, with both events occurring during the end stages of the previously-interpreted eclogite-facies history (425–400 Ma).

The younger zircon population (ca. 402 Ma) may represent (re)crystallization at HP during the early stages of exhumation and retrogression. The use of Eu anomaly to assess zircon (re)crystallization pressure is limited by the maximum pressure stability of plagioclase at ~ 1.6 GPa (depending on temperature and bulk composition), well below coesite stability (Bohlen and Boettcher, 1982; Bose and Ganguly, 1995). Thus, these results may record HP events rather than parts of the UHP history. A recent study of variably deformed felsic leucosomes and dikes across the WGR revealed an overlap in the youngest eclogite ages and the oldest melt-crystallization ages, suggesting that the younger zircon population detected in this study may be recording (re)crystallization during retrogression (Kylander-Clark and Hacker, 2014). Moreover, the minor population of zircon dates from both localities that cluster between ca. 398–396 Ma (n=7; Tables 2 and 3) may also reflect this subsequent (re)crystallization during exhumation at garnet-stable conditions. Regardless, the results from the southern and central UHP domains provide evidence for at least two eclogite-facies metamorphic events, revealing a shorter timescale of (U)HP metamorphism in comparison to previous studies that suggested a >20 Myr long-term residence at eclogite-facies depths for a large portion of the WGR (Kylander-Clark et al., 2007, 2009).

6. Conclusions

This study combines high-spatial resolution (LASS) and high-precision (ID-TIMS-TEA) techniques on the same zircon from two UHP eclogites within the Western Gneiss Region of Norway. The results capture metamorphism from 409.6 ± 0.6 Ma to 401.3 ± 0.4 Ma and 409.0 ±

0.4 Ma to 401.4 ± 0.2 Ma, with the data suggesting two (U)HP zircon (re)crystallization events at ca. 409–407 Ma and ca. 402 Ma. Trace-element analyses from both populations of zircon show flat, depleted HREE signatures and weak negative Eu anomalies interpreted to represent metamorphism under eclogite-facies conditions during these two events. Zircon and garnet trace-element abundances yield distribution coefficients that imply equilibrium between the two minerals. This study highlights the utility of coupled high-precision ID-TIMS and high-spatial resolution LASS zircon studies of eclogites across the WGR to test models for the subduction and exhumation of the WGR during the Scandian orogeny.

Acknowledgements

This work was supported by NSF Grants EAR-1019709, -1062187 (Gordon), and -1219942 (Hacker). High-precision mass spectrometry at MIT is possible because of an Instrumentation and Facilities grant (EAR-0931839 to S.A.B) and the collective sharing of knowledge by the EARTHTIME community. Thanks to Jahan Ramezani for providing assistance in the MIT Isotope Laboratory. Helpful reviews from F. Corfu and H. Brueckner greatly improved the manuscript.

References

Andersen, T.B., Jamtveit, B., Dewey, J.F., Swensson, E. (1991), Subduction and eduction of continental crust: major mechanisms during continent-continent collision and orogenic extensional collapse, a model based on the south Norwegian Caledonides. *Terra Nova*, **3**, 303-310, http://dx.doi.org/10.1111/j.1365-3121.1991.tb00148.x.

Andersen, T.B., Berry, H.B. IV, Lux, D.R., and Andresen, A. (1998), The tectonic significance of pre-Scandian $^{40}Ar/^{39}Ar$ phengite cooling ages in the Caledonides of western Norway. *Geological Society [London] Journal*, **155**, 297–309, http://dx.doi.org/10.1144/-gsjgs.155.2.0297.

Austrheim, H. (1987), Eclogitization of lower crustal granulites by fluid migration through shear zones. *Earth Planet. Sci. Lett.*, **81**, 221–232, http://dx.doi.org/10.1016/0012-821X(87)90158-0.

Austrheim, H. (1998), The influence of fluid and deformation on metamorphism of the deep crust and consequences for the geodynamics of collision zones. In: Hacker, B., Liou, J.G. (Eds.), When Continents Collide: Geodynamics and Geochemistry of Ultrahigh Pressure Rocks, *Chapman & Hall*, 297–323, http://dx.doi.org/10.1007/978-94-015-9050-1_12.

Austrheim, H., Corfu, F., Bryhni, I., Andersen, T.B. (2003), The Proterozoic Hustad igneous complex: a low strain enclave with a key to the history of the Western Gneiss Region of Norway. *Precambrian Res.*, **120**, 149–175, http://dx.doi.org/10.1016/S0301-9268(02)00167-5.

Auzzanneau, E., Vielzeuf, D., Schmidt, M.W. (2006), Experimental evidence of decompression melting during exhumation of subducted continental crust. *Contrib. Mineral. Petrol.*, **152**, 125–148, http://dx.doi.org/10.1007/s00410-006-0104-5.

Baldwin, S.L., Monteleone, B., Webb, L.E., Fitzgerald, P.G., Grove, M., and Hill, E.J. (2004), Pliocene eclogite exhumation at plate tectonic rates in eastern Papua New Guinea, *Nature,* **431**, 263–267, http://dx.doi.org/10.1038/nature02846.

Beckman, V., Möller, C., Söderlund, U., Corfu, F., Pallon, J. & Chamberlain, K. R. (2014), Metamorphic zircon formation at the transition from gabbro to eclogite in Trollheimen–

Surnadalen, Norwegian Caledonides. In: Corfu, F., Gasser, D. & Chew, D. M. (Eds.), New Perspectives on the Caledonides of Scandinavia and Related Areas. *Geological Society of London Special Publications*, **390**, 403–424, http://dx.doi.org/10.1144/SP390.26.

Bingen, B., Austrheim, H., Whitehouse, M.J., Davis, W.J. (2004), Trace element signature and U–Pb geochronology of eclogite-facies zircon, Bergen Arcs, Caledonides of W Norway. *Contrib. Mineral. Petrol.*, **147**, 671–683, http://dx.doi.org/10.1007/s00410-004-0585-z.

Bohlen, S.R., Boettcher, A.L. (1982), The quartz–coesite transformation: a precise determination and the effects of other components, *J. Geophys. Res.*, **87**, 7073–7078, http://dx.doi.org/-10.1029/JB087iB08p07073.

Bose, K., Ganguly, J. (1995), Quartz–coesite transition revisited: reversed experimental determination at 500–1200 ºC and retrieved thermochemical properties, *Am. Mineral.*, **80**, 231–238.

Bowring, J.F., McLean, N.M., Bowring, S.A. (2011), Engineering cyber infrastructure for U–Pb geochronology: Tripoli and U–Pb redux. *Geochem., Geophys., Geosyst.*, **12**, Q0AA19, http://dx.doi.org/10.1029/2010GC003479.

Brueckner, H. K. (1972), Interpretation of Rb-Sr Ages from the Precambrian and Paleozoic rocks of southern Norway. *American Journal of Sciences*, **272-4**, 334-358, http://dx.doi/10.2475/ajs.272.4.334.

Brueckner, H. K. (1979), Precambrian ages from the Geiranger-Tafjord-Grotli area of the Basal Gneiss Region, west Norway. *Norsk Geologisk Tidsskrift*, **59**, 141-153, ISSN 0029-196X.

Brueckner, H.K., van Roermund, H.L.M. (2004), Dunk tectonics: a multiple subduction/eduction model for the evolution of the Scandinavian Caledonides. *Tectonics*, **23**, TC2004, http://dx.doi.org/10.1029/2003TC001502.

Buick, I.S., Hermann, J., Williams, I.S., Gibson, R.L., Rubatto, D. (2006), A SHRIMP U-Pb and LASS trace element study of the petrogenesis of garnet-cordierite-orthoamphibole gneisses from the Central Zone of the Limpopo Belt, South Africa. *Lithos*, **88**, 150-172, http://dx.doi.org/10.1016/j.lithos.2005.09.001.

Butler, J.P., Jamieson, R.A., Steenkamp, H.M., Robinson, P. (2013), Discovery of coesite–eclogite from the Nordøyane UHP domain, Western Gneiss Region, Norway: field relations, metamorphic history, and tectonic significance. *J. Metamorph. Geol.*, **31**, 147–163, http://dx.doi.org/10.1111/jmg.12004.

Carswell, D.A., Harvey, M.A. (1985), The intrusive history and tectonometamorphic evolution of the Basal Gneiss Complex in the Moldefjord area, west Norway. In: Gee, D.G, Sturt, B.A, (Eds.), The Caledonide Orogen—Scandinavia and related areas, *Wiley*, Chichester, UK, 843–858.

Carswell, D.A., Tucker, R.D., O'Brien, P.J., Krogh, T.E. (2003a), Coesite inclusions and the U-Pb age of zircons from the Hareidland Eclogite in the Western Gneiss Region of Norway. *Lithos*, **67**, 181–190, http://dx.doi.org/10.1016/S0024-4937(03)00014-8.

Carswell, D.A., Brueckner, H.K., Cuthbert, S.J., Mehta, K., O'Brien, P.J. (2003b), The timing of stabilisation and exhumation rate for ultrahigh-pressure rocks in the Western Gneiss Region of Norway. *J. Metamorph. Geol.*, **21**, 601–612, http://dx.doi.org/10.1046/j.1525-1314.2003.00467.x.

Carswell, D.A., Cuthbert, S.J. (2003), Ultrahigh pressure metamorphism in the Western Gneiss Region of Norway. In: Carswell, D.A., Compagnoni, R. (Eds.), Ultrahigh pressure metamorphism, *EMU Notes in Mineralogy*, **5**, 51–73.

Carswell, D.A., van Roermund, H.L.M., Wiggers de Vries, D.F. (2006), Scandian ultrahigh-pressure metamorphism of Proterozoic basement rocks on Fjørtoft and Otrøy, Western Gneiss Region, Norway. *International Geology Review*, **48**, 957–977, http://dx.doi.org/10.2747/0020-6814.48.11.957.

Corfu F., Hanchar J.M., Hoskin P.W.O., Kinny P. (2003), Atlas of zircon textures. In: Hanchar, J.M. and Hoskin P.W.O. (eds.), Zircon. *Reviews in Mineralogy and Geochemistry*, **53**, 468–500. Washington, DC: Mineralogical Society of America.

Corfu, F., Austrheim, H. Ganzhorn, A.C. (2013), Localized granulite and eclogite facies metamorphism at Flatraket and Kråkeneset, Western Gneiss Region: U-Pb data and tectonic implications. *Geological Society of London Special Publications*, **390**, 425–442, http://dx.doi.org/10.1144/SP390.22.

Cuthbert, S.J., Carswell, D.A. (1990), Formation and exhumation of medium-temperature eclogites in the Scandinavian Caledonides. In: Carswell, D.A. (eds.), Eclogite Facies Rocks, *Chapman and Hall*, New York, 180–203.

Cuthbert, S.J., Carswell, D.A., Krogh-Ravna, E.J., Wain, A. (2000), Eclogites and eclogites in the Western Gneiss Region, Norwegian Caledonides. *Lithos*, **52**, 165–195, http://dx.doi.org/10.1016/S0024-4937(99)00090-0.

Dobrzhinetskaya, L.F., Eide, E.A., Larsen, R.B., Sturt, B.A., Trønnes, R.G., Smith, D.C., Taylor, W.R., Posukhova, T.V. (1995), Microdiamond in high-grade metamorphic rocks of the Western Gneiss region, Norway. *Geology*, **23**, 597–600, http://dx.doi.org/10.1130/0091-7613(1995) 023<0597:MIHGMR> 2.3.CO;2.

Engvik, A.K., Austrheim, H., Andersen, T.B. (2000), Structural, mineralogical and petrophysical effects on deep crustal rocks of fluid-limited polymetamorphism, Western Gneiss Region, Norway. *Geological Society [London] Journal*, **157**, 121–134, http://dx.doi.org/-10.1144/jgs.157.1.121.

Gáal, G., Gorbatschev, R. (1987), An outline of the Precambrian evolution of the Baltic shield. *Precambrian Research*, **35**, 15–52, http://dx.doi.org/10.1016/0301-9268(87)90044-1.

Gebauer, D., Lappin, M.A., Grünenfelder, M., Wyttenbach, A. (1985), The age and origin of some Norwegian eclogites: a U–Pb zircon and REE study. *Chem. Geol.*, **52**, 227–247, http://dx.doi.org/10.1016/0168-9622(85)90020-X.

Glodny, J., Kühn, A., Austrheim, H. (2008), Diffusion v. recrystallization processes in Rb–Sr geochronology: isotopic relicts in eclogite facies rocks, Western Gneiss Region, Norway. *Geochim. et Cosmochim. Acta.*, **72**, 506–525, http://dx.doi.org/10.1016/j.gca.2007.10.021.

Griffin, W.L., H.K. Brueckner (1980), Caledonian Sm-Nd ages and a crustal origin for Norwegian eclogites, *Nature*, **285**, 319–321, http://dx.doi.org/10.1038/285319a0.

Griffin, W.L., Brueckner, H.K. (1985), REE, Rb-Sr and Sm-Nd studies of Norwegian eclogites. *Chem. Geol.*, **52**, 249–271, http://dx.doi.org/10.1016/0168-9622(85)90021-1.

Griffin, W.L., Austrheim, H., Brastad, K., Bryhni, I., Krill, A.G., Krogh, E.J., Mørk, M.B.E., Qvale, H., Tørudbakken, B. (1985), High-pressure metamorphism in the Scandinavian Caledonides. In: Gee, D.G, Sturt, B.A, (Eds.), The Caledonide Orogen—Scandinavia and related areas, *Wiley*, Chichester, UK, 783-801.

Gordon, S. M., Whitney, D. L., Teyssier, C. & Fossen, H. (2013), U–Pb dates and trace-element geochemistry of zircon from migmatite, Western Gneiss Region, Norway: significance for history of partial melting in continental subduction. *Lithos*, **170–171**, 35–53, http://dx.doi.-org/10.1016/j.lithos.2013.02.003.

Hacker, B.R. (2007), Ascent of the ultrahigh-pressure Western Gneiss Region, Norway. In: Cloos, M., W.D. Carlson, M.C. Gilbert, J.G. Liou, and S.S. Sorenson (Eds.), Convergent Margin Terranes and Associated Regions, A Tribute to W.G. Ernst, *Geological Society of America Special Paper,* **419,** 171–184, Geological Society of America, Boulder, CO, http://dx.doi.org/10.1130/2006.2419(09).

Hacker, B.R., Gans, P.B. (2005), Continental collisions and the creation of ultrahigh-pressure terranes: Petrology and thermochronology of nappes in the central Scandinavian Caledonides. *Geological Society of America Bulletin*, **117**, 117–134, http://dx.doi.org/-10.1130/B25549.1.

Hacker, B.R., Andersen, T.B., Johnston, S., Kylander-Clark, A.R.C., Peterman, E.M., Walsh, E.O., Young, D. (2010), High-temperature deformation during continental-margin subduction & exhumation: the ultrahigh-pressure Western Gneiss Region of Norway. *Tectonophysics*, **480(1–4)**, 149–171. doi:http://dx.doi.org/10.1016/j.tecto.2009.08.012.

Harley, S.L., Kinny, P., Snape, I., Black, L.P. (2001), Zircon chemistry and the definition of events in Archean granulite terrains. In: Fourth International Archean Symposium, Extended Abstract Volume, *AGSO Geoscience Australia Record*, 2001/37, 511-513.

Harley, S.L., Kelly, N.M. (2007), The impact of zircon-garnet REE distribution data on the interpretation of zircon U-Pb ages in complex high-grade terrains: An example from the Rauer Islands, East Antarctica. *Chem. Geol.*, **241**, 62-87, http://dx.doi.org/-10.1016/j.chemgeo.2007.02.011.

Hermann, J., Rubatto, D. (2003), Relating zircon and monazite domains to garnet growth zones: Age and duration of granulite facies metamorphism in the Val Malenco lower crust. *J. Metamorph. Geol.*, **21**, 833-852, http://dx.doi.org/10.1046/j.1525-1314.2003.00484.x.

Hinton, R., Upton, B. (1991), The chemistry of zircon: variations within and between large crystals from syenite and alkali basalt xenoliths. *Geochim. et Cosmochim. Acta.*, **55**, 3287–3302, http://dx.doi.org/10.1016/0016-7037(91)90489-R.

Hokada, T., Harley, S.L. (2004), Zircon growth in UHT leucosome: Constraints from zircon-garnet rare earth elements (REE) relations in Napier Complex, East Antarctica. *J. Mineral. Petrol. Sciences*, **99**, 180-190, http://dx.doi.org/10.2465/jmps.99.180.

Hoskin, P.W.O., Ireland, T.R. (2000), Rare earth element chemistry of zircon and its use as a provenance indicator. *Geology*, **28**, 627–630, http://dx.doi.org/10.1130/0091-7613(2000)28<627:REECOZ> 2.0.CO;2.

Hoskin, P.W.O., Schaltegger, U. (2003), The composition of zircon and igneous and metamorphic petrogenesis. *Rev. Mineral. Geochem.* **53**, 27–62, http://dx.doi.org/-10.2113/0530027.

Jamtveit, B., Carswell, D.A, Mearns, E.W. (1991), Chronology of the high-pressure metamorphism of Norwegian garnet peridotites/pyroxenites, *J. Metamorph. Geol.*, **9**, 125–139, http://dx.doi.org/10.1111/j.1525-1314.1991.tb00509.x.

Kelly, N.M., Harley, S.L. (2005), An integrated microtextural and chemical approach to zircon geochronology: Refining the Archaean history of the Napier Complex, east Antarctica. *Contrib. Mineral. Petrol.*, **149**, 57-84, http://dx.doi.org/10.1007/s00410-004-0635-6.

Krogh, E.J. (1977), Evidence for Precambrian continent-continent collision in western Norway. *Nature*, **267**, 17-19, http://dx.doi.org/10.1038/267017a0.

Krogh, E.J. (1982), Metamorphic evolution of Norwegian country-rock eclogites, as deduced from mineral inclusions and compositional zoning in garnets. *Lithos*, **15**, 305-321, http://dx.doi.org/10.1016/0024-4937(82)90021-4.

Krogh, T.E. (1982), Improved accuracy of U–Pb zircon dating by creation of more concordant systems using air abrasion technique. *Geochim. et Cosmochim. Acta.*, **46**, 637–649, http://dx.doi.org/10.1016/0016-7037(82)90165-X.

Krogh, T.E., Mysen, B.O., Davis, G.L. (1974), A Paleozoic age for the primary minerals of a Norwegian eclogite. Annual Report of the Geophysical Laboratory. *Carnegie Institution*, Washington, **73**, 575–576.

Krogh, T.E., Kamo, S.L., Robinson, P., Terry, M.P., Kwok, K. (2011), U–Pb zircon geochronology of eclogites from the Scandian Orogen, northern Western Gneiss Region, Norway: 14–20 million years between eclogite crystallization and return to amphibolite-facies conditions. *Can. J. Earth Sciences*, **48(2)**, 441–472, http://dx.doi.org/10.1139/E10-076.

Kylander-Clark, A.R.C., Hacker, B.R. (in press), Age and significance of felsic dikes from the UHP western gneiss region. *Tectonics*, http://dx.doi.org/10.1002/2014TC003582.

Kylander-Clark, A.R.C., Hacker, B.R., Johnson, C.M., Beard, B.L., Mahlen, N.J., Lapen, T.J. (2007), Coupled Lu–Hf and Sm–Nd geochronology constrains prograde and exhumation histories of high- and ultrahigh-pressure eclogites from western Norway. *Chem. Geol.*, **242(1–2)**, 137–154, http://dx.doi.org/10.1016/j.chemgeo.2007.03.006.

Kylander-Clark, A.R.C., Hacker, B.R., Mattinson, J.M. (2008), Slow exhumation of UHP terranes: titanite and rutile ages of the Western Gneiss Region, Norway. *Earth Planet. Sci. Lett.*, **272(3-4)**: 531–540, http://dx.doi.org/10.1016/j.epsl.2008.05.019.

Kylander-Clark, A.R.C., Hacker, B.R., Johnson, C.M., Beard, B.L., Mahlen, N.J. (2009), Slow subduction and rapid exhumation of a thick ultrahigh-pressure terrane. *Tectonics*, **28(2)**, TC2003, http://dx.doi.org/10.1029/2007TC002251.

Kylander-Clark, A. R. C., B.R. Hacker, C.G. Mattinson (2012), Size and exhumation rate of ultrahigh-pressure terranes linked to orogenic stage, *Earth Planet. Sci. Lett.*, **321–322**, 115–120, http://dx.doi.org/10.1016/j.epsl.2011.12.036.

Kylander-Clark, A.R.C., Hacker, B.R., Cottle, J.M., (2013), Laser-ablation split-stream ICP petrochronology. *Chem. Geol.*, **345**, 99–112, http://dx.doi.org/10.1016/j.chemgeo.-2013.02.019.

Labrousse, L., Jolivet, L., Andersen, T.B., Agard, P., Hébert, R., Maluski, H., Schärer, U. (2004), Pressure–temperature–time-deformation history of the exhumation of ultrahigh-pressure rocks in the Western Gneiss region, Norway. In: Whitney, D.L., Teyssier, C., Siddoway, C.S. (Eds.), Gneiss Domes in Orogeny, *Geological Society of America Special Paper*, **380**, 155–183, Geological Society of America, Boulder, CO, http://dx.doi.org/10.1130/0-8137-2380-9.155.

Labrousse, L., G. Prouteau, A.C. Ganzhorn (2011), Continental exhumation triggered by partial melting at ultrahigh pressure, *Geology*, **39**, 1171–1174, http://dx.doi.org/10.1130/-G32316.1.

Lappin, M.A., Smith, D.C. (1978), Mantle-equilibrated orthopyroxene eclogite pods from the Basal Gneisses in the Selje District, western Norway. *J. Petrol.*, **19**, 530–584, http://dx.doi.org/10.1093/petrology/19.3.530.

Mattinson, J.M. (2005), Zircon U-Pb chemical abrasion (“CA-TIMS”) method: combined annealing and multi-step partial dissolution analysis for improved precision and accuracy of zircon ages, *Chem. Geol.*, **220**, 47–66, http://dx.doi.org/10.1016/j.chemgeo.2005.03.011.

Mattinson, C.G., Wooden, J.L., Liou, J.G., Bird, D.K., Wu, C.L. (2006), Age and duration of eclogite-facies metamorphism, North Qaidam HP/UHP terrane, Western China. *Amer. J. Science*, **306**, 683–711, http://dx.doi.org/10.2475/09.2006.01

McClelland, W.C., Power, S.E., Gilotti, J.A., Mazdab, F.K., and Wopenka, B. (2006), U-Pb SHRIMP geochronology and trace element geochemistry of coesite-bearing zircons, North-East Greenland Caledonides, In: Hacker, B.R., McClelland, B., and Liou, J.G. (Eds.) Ultrahigh-Pressure Metamorphism: Deep Continental Subduction: *Geological Society of America Special Paper*, **403**, 23–43, Geological Society of America, Boulder, CO, http://dx.doi.org/10.1130/2006.2403(02).

McLean, N.M., Bowring, J.F., Bowring, S.A. (2011), An algorithm for U-Pb isotope dilution data reduction and uncertainty propagation, *Geochem. Geophys. Geosyst.*, **12**, Q0AA18, http://dx.doi.org/10.1029/2010GC003478.

Mearns, E. W. (1986), Sm-Nd ages for Norwegian garnet peridotite, *Lithos*, **19**, 269–278, http://dx.doi.org/10.1016/0024-4937(86)90027-7.

Monteleone, B.D., Baldwin, S.L., Webb, L.E., Fitzgerald, P.G., Grove, M., Schmitt, A.K. (2007), Late Miocene–Pliocene eclogite facies metamorphism, D'Entrecasteaux Islands, SE Papua New Guinea, *J. Metamorph. Geol.*, **25**, 245–265, http://dx.doi.org/10.1111/j.1525-1314.2006.00685.x.

Mørk, M.B.E., Mearns, E.W. (1986), Sm-Nd isotopic systematics of a gabbro-eclogite transition, *Lithos*, **19**, 255–267, http://dx.doi.org/10.1016/0024-4937(86)90026-5.

Mundil R., Metcalfe I., Ludwig K.R., Renne P.R., Oberli F., Nicoll, R.S. (2001), Timing of the Permian–Triassic biotic crisis: Implications from new zircon U-Pb age data (and their limitations). *Earth Planet. Sci. Lett.*, **187**, 131–145, http://dx.doi.org/10.1016/S0012-821X(01)00274-6.

Mysen, B.O. (1972), Five Clinopyroxenes in the Hareidland eclogite, Western Norway. *Contrib. Mineral. Petrol.*, **34**, 315–325, http://dx.doi.org/10.1007/BF00373761.

Mysen, B.O., Heier, K.S. (1972), Petrogenesis of eclogites in high-grade metamorphic gneisses exemplified by the Hareidland eclogite, west Norway. *Contrib. Mineral. Petrol.*, **36**, 73– 94, http://dx.doi.org/10.1007/BF00372836.

Peterman, E.M., Hacker, B.R., Baxter, E.F. (2009), Phase transformations of continental crust during subduction and exhumation: Western Gneiss Region, Norway. *Eur. J. Mineral.*, **21**, 1097–1118, http://dx.doi.org/10.1127/0935-1221/2009/0021-1988.

Ravna, E.J.K., Terry, M.P. (2004), Geothermobarometry of UHP and HP eclogites and schists–an evaluation of equilibria among garnet–clinopyroxene–kyanite–phengite–coesite/quartz. *J. Metamorph. Geol.*, **22**, 579–592, http://dx.doi.org/10.1111/j.1525-1314.2004.00534.x.

Renedo, R.N., Nachlas, W.O., Whitney, D.L., Teyssier, C., Piazolo, S., Gordon, S.M., Fossen, H. (in press), Fabric development during exhumation from ultrahigh-pressure in an eclogite-bearing shear zone, Western Gneiss Region, Norway. *J. Struct. Geol.*, http://dx.doi.org/-10.1016/j.jsg.2014.09.012.

Roberts, D. (2003), The Scandinavian Caledonides: Event chronology, palaeogeographic settings and likely modern analogues. *Tectonophysics*, **365**, 283–299, http://dx.doi.org/10.1016/-S0040-1951(03)00026-X.

Roberts, D., Gee, D.G. (1985), An introduction to the structure of the Scandinavian Caledonides. In: Gee, D.G, Sturt, B.A, (Eds.), The Caledonide Orogen—Scandinavia and related areas, *Wiley*, Chichester, UK, 55– 68.

Robinson, P. (1995). Extension of Trollheimen tectono-stratigraphic sequence in deep synclines near Molde and Brattvåg, Western Gneiss Region, southern Norway. *Norsk Geologisk Tidsskrift*, **75**, 181–198.

Røhr, T.S., Corfu, F., Austrheim, H., Andersen, T.B. (2004), Sveconorwegian U–Pb zircon and monazite ages of granulite-facies rocks, Hisarøya Gulen, Western Gneiss Region, Norway. *Norwegian J. Geol.*, **84**, 251–256, ISSN 029-196X.

Røhr, T.S., Bingen, B., Robinson, P., Reddy, S.M. (2013), Geochronology of Paleoproterozoic augen gneisses in the Western Gneiss Region, Norway: evidence for Sveconorwegian zircon neocrystallization and Caledonian zircon deformation. *J. Geol.*, **121**, 105–128, http://-dx.doi.org/10.1086/669229

Root, D.B., Hacker, B.R., Mattinson, J.M., Wooden, J.L. (2004), Zircon geochronology and ca. 400 Ma exhumation of Norwegian ultrahigh-pressure rocks: an ion microprobe and chemical abrasion study. *Earth Planet. Sci. Lett.*, **228**, 325–341, http://dx.doi.org/10.1016/-j.epsl.2004.10.019.

Root, D.B., Hacker, B.R., Gans, P.B., Ducea, M.N., Eide, E.A., Mosenfelder, J.L. (2005), Discrete ultrahigh-pressure domains in the Western Gneiss Region, Norway: implications for formation and exhumation. *J. Metamorph. Geol.*, **23**, 45–61, http://dx.doi.org/10.1111/-j.1525-1314.2005.00561.x.

Rubatto, D. (2002), Zircon trace element geochemistry: distribution coefficients and the link between U–Pb ages and metamorphism. *Chem. Geol.*, **184**, 123–138, http://dx.doi.org/-10.1016/S0009-2541(01)00355-2.

Rubatto, D., Hermann, J. (2003), Zircon formation during fluid circulation in eclogites (Monviso, Western Alps): implications for Zr and Hf budget in subduction zones. *Geochim. et Cosmochim. Acta.*, **67**, 2173–2187, http://dx.doi.org/10.1016/S0016-7037(02)01321-2.

Rubatto, D., Hermann, J., Buick, I.S. (2006), Temperature and bulk composition control on the growth of monazite and zircon during low-pressure anatexis (Mount Stafford, central Australia). *J. Petrol.*, **47**, 1973–1996, http://dx.doi.org/10.1093/petrology/egl033.

Rubatto, D., Hermann, J. (2007a), Zircon behaviour in deeply subducted rocks, *Elements*, **3**, 31–35, http://dx.doi.org/10.2113/gselements.3.1.31.

Rubatto, D., Hermann, J. (2007b), Experimental zircon/melt and zircon/garnet trace element partitioning and implications for the geochronology of crustal rocks. *Chem. Geol.*, **241**, 38-61, http://dx.doi.org/10.1016/j.chemgeo.2007.01.027.

Scambelluri, M., Pettke, T., van Roermund, H.L.M. (2008), Majoritic garnets monitor deep subduction fluid flow and mantle dynamics. *Geology*, **36**, 59–62. http://dx.doi.org/-10.1130/G24056A.1.

Schärer, U., Labrousse, L. (2003), Dating the exhumation of UHP rocks and associated crustal melting in the Norwegian Caledonides, *Contrib. Mineral. Petrol.*, **144**, 758–770, http://-dx.doi.org/10.1007/s00410-002-0428-8.

Schaltegger, U., Fanning, C.M., Günther, D., Maurin, J.C., Schulmann, K., Gebauer, D. (1999), Growth, annealing and recrystallization of zircon and preservation of monazite in high-grade metamorphism: conventional and in situ U–Pb isotope, cathodoluminescence and microchemical evidence. *Contrib. Mineral. Petrol.*, **134**, 186–201, http://dx.doi.org/10.1007/-s004100050478.

Schoene, B., C. Latkoczy, U. Schaltegegger, and D. Günther (2010), A new method integrating high-precision U–Pb geochronology with zircon trace-element analysis (U–Pb TIMS-TEA), *Geochim. et Cosmochim. Acta.*, **74**, 7144–7159, http://dx.doi.org/10.1016/j.gca.2010.09.016.

Schoene, B. (2013), U-Th-Pb Geochronology. In: Rudnick, R. (Eds.), Treatise on Geochemistry 2nd edition, *Elsevier*, **4.10**, 341–378, http://dx.doi.org/10.1016/B978-0-08-095975-7.00310-7

Skår, Ø. (2000), Field relations and geochemical evolution of the Gothian rocks in the Kvamsøy area, southern Western Gneiss Complex, Norway. *Nor. Geol. Unders. Bull*. **437**, 5–23.

Skår, Ø., Furnes, H., Claesson, S. (1994), Middle Proterozoic magmatism within the Western Gneiss Region, Sunnfjord, Norway. *Norsk Geol. Tidsskr.*, **74**, 114–126, ISSN 0029-196X.

Skår, Ø., Pedersen, R.B. (2003), Relations between granitoid magmatism and migmatization: U–Pb geochronological evidences from the Western Gneiss Complex, Norway. *Geological Society [London] Journal*, **160**, 935–946, http://dx.doi.org/10.1144/0016-764901-121.

Smith, D.C. (1984), Coesite in clinopyroxene in the Caledonides and its implications for geodynamics. *Nature*, **310**, 641–644, http://dx.doi.org/10.1038/310641a0.

Smith, D.C. (1988), A review of the peculiar mineralogy of the “Norwegian coesite-eclogite province”, with crystal-chemical, petrological, geochemical and geodynamical notes and an extensive bibliography. In: Smith, D.C. (Eds.), “Eclogites and eclogite-facies rocks”. *Elsevier*, 1-206.

Smith, D.C., Godard, G. (2013), A Raman spectroscopic study of diamond and disordered sp3-carbon in the coesite-bearing Straumen eclogite pod, Norway. *J. Metamorph. Geol.*, **31**, 19–33, http://dx.doi.org/10.1111/jmg.12007.

Spencer, K.J., Hacker, B.R., Kylander-Clark, A.R.C., Andersen, T.B., Cottle, J.M., Stearns, M.A., Poletti, J.E., Seward, G.G.E. (2013), Campaign style titanite U–Pb dating by laser-ablation ICP: implications for crustal flow, phase transformations and titanite closure. *Chem. Geol.*, **341**, 84–101, http://dx.doi.org/10.1016/j.chemgeo.2012.11.012.

Spengler, D., Brueckner, H.K., van Roermund, H.L.M., Drury, M.R., Mason, P.R.D. (2009), Long-lived, cold burial of Baltica towards 200 km depth. *Earth Planet. Sci. Lett.*, **281**, 27–35, http://dx.doi.org/10.1016/j.epsl.2009.02.001.

Stephens, M.B., Gee, D.G. (1989), Terranes and polyphase accretionary history in the Scandinavian Caledonides. *Geol. Soc. Am. Spec.* Paper, **230**, 17– 30, Geological Society of America, Boulder, CO, http://dx.doi.org/10.1130/SPE230-p17.

Straume, A.K., Austrheim, H. (1999), Importance of fracturing during retro-metamorphism of eclogites. *J. Metamorph. Geol.*, **17**, 637–652, http://dx.doi.org/10.1046/j.1525-1314.1999.00218.x.

Sun S.S., McDonough, W.F. (1989), Chemical and isotopic systematics of oceanic basalts: implications for mantle composition and processes, *Geological Society of London Special Publications*, **42**, 313–345, http://dx.doi.org/10.1144/GSL.SP.1989.042.01.19.

Taylor, R.J.M., Harley, S.L., Hinton, R.W., Elphick, S., Clark, C., Kelly, N.M. (2014), Experimental determination of REE partition coefficients between zircon, garnet, and melt: a key to understanding high-temperature crustal processes. *J. Metamorph. Geol.*, http://-dx.doi.org/10.1111/jmg.12118.

Terry, M.P., Robinson, P., Ravna, E.J.K. (2000a), Kyanite eclogite thermobarometry and evidence for thrusting of UHP over HP metamorphic rocks, Nordøyane, Western Gneiss Region, Norway. *Amer. Mineral.*, **85**, 1637–1650.

Terry, M.P., Robinson, P., Hamilton, M.A., Jercinovic, M.J. (2000b), Monazite geochronology of UHP and HP metamorphism, deformation, and exhumation, Nordøyane, Western Gneiss Region, Norway, *Amer. Mineral.*, **85**, 1651–1664.

Tucker, R.D., Robinson, P., Solli, A., Gee, D.G., Thorsnes, T., Krogh, T.E., Nordgulen, Ø., Bickford, M.E. (2004), Thrusting and extension in the Scandian hinterland, Norway: New U–Pb ages and tectonostratigraphic evidence. *Amer. J. Science*, **304(6)**, 477–532, http://-dx.doi.org/10.2475/ajs.304.6.477.

Tucker, R.D., Krogh, T.E., Råheim, A. (1990), Proterozoic evolution and age-province boundaries in the central part of the Western Gneiss Region, Norway. Results of U–Pb dating of accessory minerals from Trondheimsfjord to Geiranger. In Mid- Proterozoic Laurentia–Baltica. Edited by C.F. Gower, A.B. Ryan, and T. Rivers. *Geological Association of Canada, Special Paper*, **38**, 149–173.

Van Roermund, H.L.M. (2009), Recent progress in Scandian UHPM in the northernmost domain of the Western Gneiss Complex, SW Norway: continental subduction down to 180–200 km. *Geological Society [London] Journal*, **166**, 1–13, http://dx.doi.org/10.1144/0016-76492008-020.

Van Westrenen, W., Blundy, J., Wood, B. (1999), Crystal–chemical controls on trace element partitioning between garnet and anhydrous silicate melt. *Amer. Mineral.*, **84**, 838–847.

Vrijmoed, J.C., Van Roermund, H.L.M., Davis, G.R. (2006), Evidence for diamond-grade ultrahigh-pressure metamorphism and fluid interaction in the Svartberget Fe–Ti garnet peridotite-websterite body, Western Gneiss Region, Norway. *Mineral. Petrol.*, **88**, 381–405. http://dx.doi.org/10.1007/s00710-006-0160-6.

Vrijmoed, J.C., Smith, D.C., Van Roermund, H.L.M. (2008), Raman confirmation of microdiamond in the Svartberget Fe–Ti type garnet peridotite, Western Gneiss Region, Western Norway. *Terra Nova*, **20**, 295–301, http://dx.doi.org/10.1111/j.1365-3121.2008.00820.x.

Wain, A. (1997), New evidence for coesite in eclogite and gneisses: Defining an ultrahigh-pressure province in the Western Gneiss region of Norway. *Geology*, **25**, 927–930, http-://dx.doi.org/0.1130/0091-7613(1997) 025<0927:NEFCIE> 2.3.CO;2.

Wain, A., Waters, D., Jephcoat, A., Olijnyk, H. (2000), The high-pressure to ultrahigh-pressure transition in the Western Gneiss Region, Norway. *Eur. J. Mineral.*, **12**, 667–687, http://-dx.doi.org/10.1127/0935-1221/2000/0012-0667.

Wain, A., Waters, D., Austrheim, H. (2001), Metastability of granulites and processes of eclogitization in the UHP region of western Norway, *J. Metamorph. Geol.*, **19**, 609–625, http://dx.doi.org/10.1046/j.0263-4929.2001.00333.x.

Walsh, E.O., Hacker, B.R. (2004), The fate of subducted continental margins: two-stage exhumation of the high-pressure to ultrahigh-pressure Western Gneiss Region, Norway. *J. Metamorph. Geol.*, **22**, 671–687, http://dx.doi.org/10.1111/j.1525-1314.2004.00541.x.

Whitehouse, M.J., Platt, J.P. (2003), Dating high-grade metamorphism–Constraints from rare-earth elements in zircon and garnet. *Contrib. Mineral. Petrol.*, **145**, 61–74, http://dx.doi.org/-10.1007/s00410-002-0432-z.

Whitney, D.L., Evans, B.W., 2010. Abbreviations for names of rock-forming minerals. Am. Mineral. 95, 185–187.

Young, D.J., Hacker, B.R., Andersen, T.B., Corfu, F. (2007), Prograde amphibolite facies to ultrahigh-pressure transition along Nordfjord, western Norway: implications for exhumation tectonics. *Tectonics*, **26**, TC1007, http://dx.doi.org/10.1029/2004TC001781.

Figures:

Figure 1. (a) Generalized geologic map of the Western Gneiss Region showing the southern, central, and northern UHP domains after Hacker et al. (2010). Locations of (U)HP eclogites and their respective U-Pb zircon dates are shown. Simplified geologic maps of (b) the Ulsteinvik eclogite on Hareidlandet within the central UHP domain (after Mysen and Heier, 1972) and (c) the SW coast of Saltaneset within the southern UHP domain showing the layered eclogite within the Saltaneset mylonite zone (after Renedo et al., 2014). Stars and areas outlined mark sample localities in a, b, and c.

Figure 2. Cathodoluminescence images from the Ulsteinvik eclogite and Saltaneset garnet-quartz and omphacite layers displaying patchy- and polygonal-sector zoning, along with some rim overgrowths, preserved within the metamorphic zircon of the two samples. Corresponding ID-TIMS dates are also shown. Black lines denote microsampled fragments of Ulsteinvik z1. Omphacite layer zircon (spot 20) did not yield a Scandian ID-TIMS date; therefore, the LASS date is shown. Scale bar is 100 micrometers.

Figure 3. Concordia diagrams showing all of the Caledonian U-Pb zircon analyses from both the Ulsteinvik and Saltaneset layered eclogite: (a) individual ID-TIMS analyses; (b) LA-ICP-MS analyses. Insets show Scandian (U)HP dates from both techniques. Dates given in Ma.

Figure 4. U-Pb zircon analyses (LASS (green) and ID-TIMS (red) dates from the exact same zircon) from the two eclogites: (a) Ulsteinvik and (b) Saltaneset (see Table 2), along with additional LASS dates (blue). The numbers correspond to the laser spot (LASS) and zircon grain

or fraction (ID-TIMS). The range of single grain or fraction of a grain ID-TIMS analyses are reported as Th-corrected $^{206}Pb/^{238}U$ dates.

Figure 5. Chondrite-normalized zircon trace element data collected by LASS and color-coded by the corresponding LASS dates for (a) the Ulsteinvik eclogite, (b) the garnet–quartz layer of the Saltaneset eclogite, and (c) the omphacite-rich layer of the Saltaneset eclogite. Shaded regions show range of LASS analyses from inherited zircons. Solution ICP-MS analyses (TEA), color-coded by the corresponding ID-TIMS dates, for (d) the Ulsteinvik eclogite and (e) the combined Saltaneset eclogite garnet–quartz (G) and omphacite-rich (O) layers. LASS trace-element results from the same samples (shaded regions) are shown for comparison.

Figure 6. Chondrite-normalized garnet trace element data collected by LA-ICP-MS for (a) early-formed garnet porphyroblasts of the Ulsteinvik eclogite, (b) late-recrystallized garnet along some of the early garnet rims and within the matrix of the Ulsteinvik eclogite, (c) the omphacite-rich layer of the Saltaneset eclogite, and (d) garnet–quartz layer of the Saltaneset eclogite with Lu profile across representative zoned garnet 3.

Figure 7. Zircon/garnet partition coefficients for the different populations and/or generations of zircon (solution ICP-MS) and garnet analyses (LA-ICP-MS). Averaged zircon trace element compositions of the two age populations are paired with the average of the different garnet trace-element compositions observed in Ulsteinvik and Saltaneset eclogite layers. Also shown is the range in previously calculated experimental and empirical zircon/garnet partition coefficients discussed in the text.

Figure S1. Concordia diagrams showing U-Pb zircon results from the (a and b) Saltaneset garnet–quartz layer (NW13-02-G) and (c and d) the omphacite-rich layer (NW13-02-O) analyzed by ID-TIMS and LASS, respectively. Upper- and lower-intercept ages were calculated using the program U-Pb_Redux (Bowring et al., 2011; McLean et al., 2011). Each ellipse represents a single zircon or spot analysis and the 2-sigma uncertainties. Dates listed on concordia are in Ma.

Figure S2. Scandian zircon trace elements as a function of time. Plots are shaded for ca. 409–407 and ca. 402 Ma zircon populations. (a) Lu_N/Gd_N, Eu/Eu*, and Th/U data and (b) sum of absolute concentrations (ppm) of MREE–HREE, Y/Sc, and Zr/Hf data vs. ID-TIMS $^{206}Pb/^{238}U$ (Th-corrected) age for the Ulsteinvik eclogite, the garnet–quartz layer of the Saltaneset eclogite, and the omphacite-rich layer of the Saltaneset eclogite. Lu_N/Gd_N and Eu/Eu* analyses are normalized to chondrite values of Sun and McDonough (1989).

Figure S3. Zircon/garnet partition coefficients for the different populations and/or generations of zircon (LASS) and garnet analyses (LA-ICP-MS). Average zircon trace element compositions of the young (ca. 405–397 Ma) and old (ca. 414–406 Ma) age populations are paired with the average of the different garnet trace-element compositions observed in Ulsteinvik and Saltaneset eclogite layers. Also shown is the range in previously published experimental and empirical zircon/garnet partition coefficients discussed in the text.

List of Tables

Table 1. Geochronological summary of various Scandian (U)HP eclogites from the Western Gneiss Region

Table 2. Zircon U-Th-Pb LA-ICP-MS isotopic data from the Western Gneiss Region: Ulsteinvik and Saltaneset eclogites

Table 3. Zircon U-Pb ID-TIMS isotopic data from the Western Gneiss Region: Ulsteinvik and Saltaneset eclogites

Table 4. Zircon LASS and solution ICP-MS trace-element data from the Western Gneiss Region: Ulsteinvik and Saltaneset eclogites

Table 5. Garnet LA-ICP-MS trace-element data and calculated zircon–garnet partition coefficients from the Western Gneiss Region: Ulsteinvik and Saltaneset eclogites

Appendix: Laser-ablation split stream, U-Pb ID-TIMS, and ID-TIMS-TEA methodology.

Figure 1

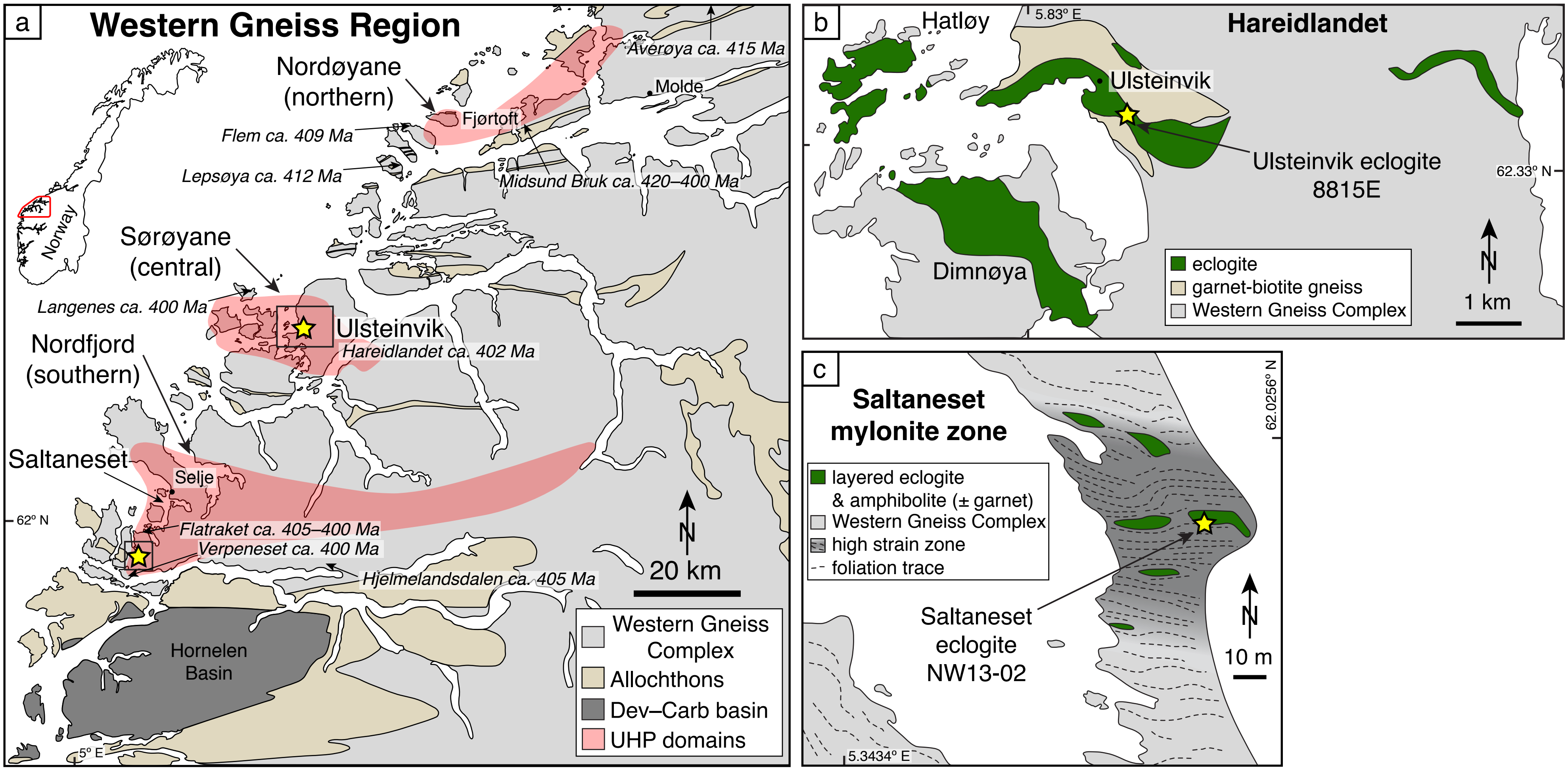

DesOrmeau et al. Figure 1

Figure 2

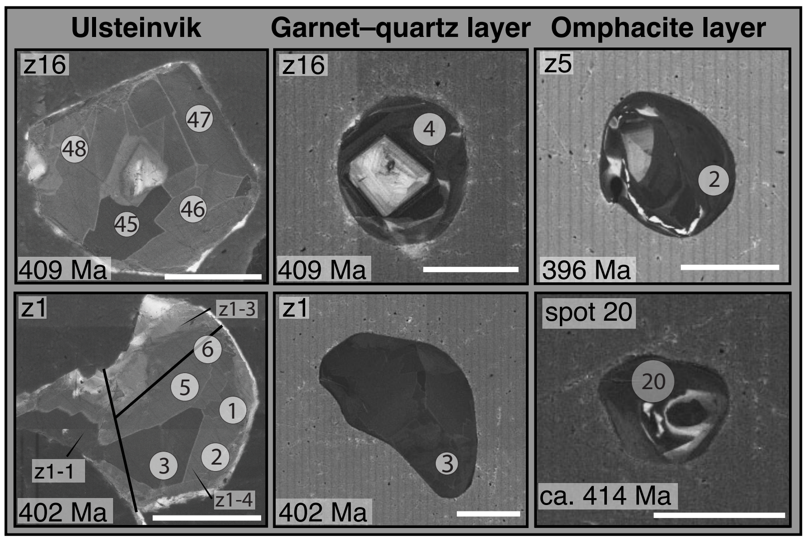

DesOrmeau et al. Figure 2

Figure 3

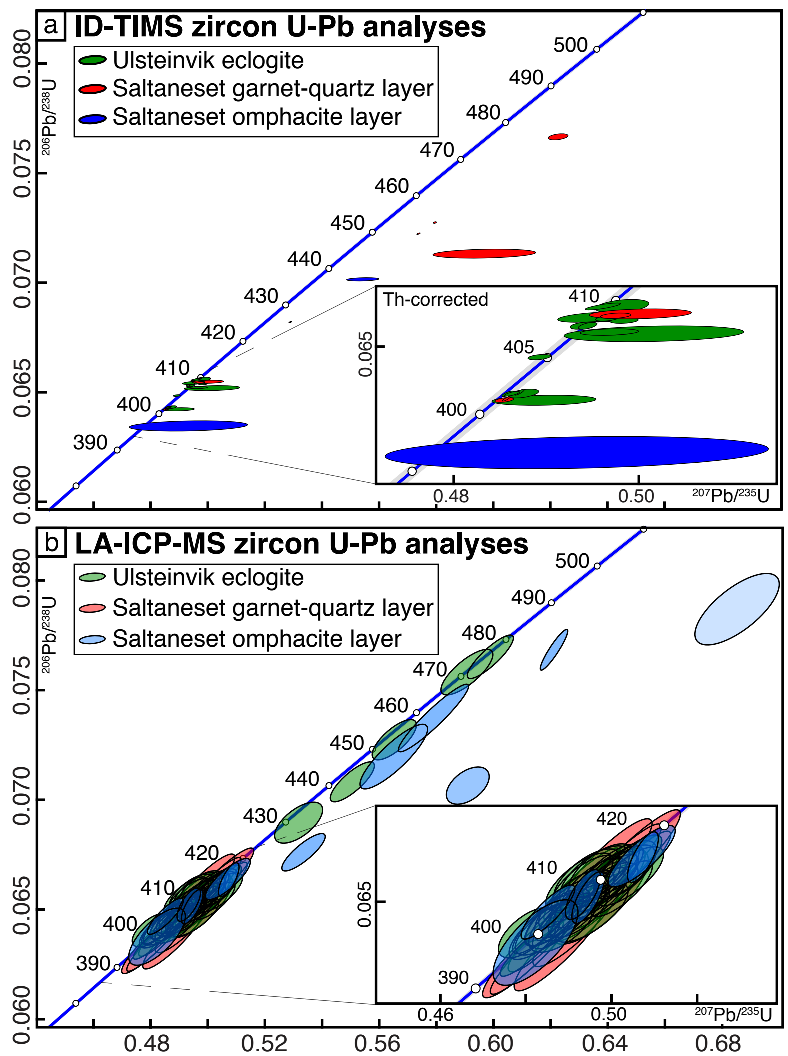

DesOrmeau et al. Figure 3

Figure 4

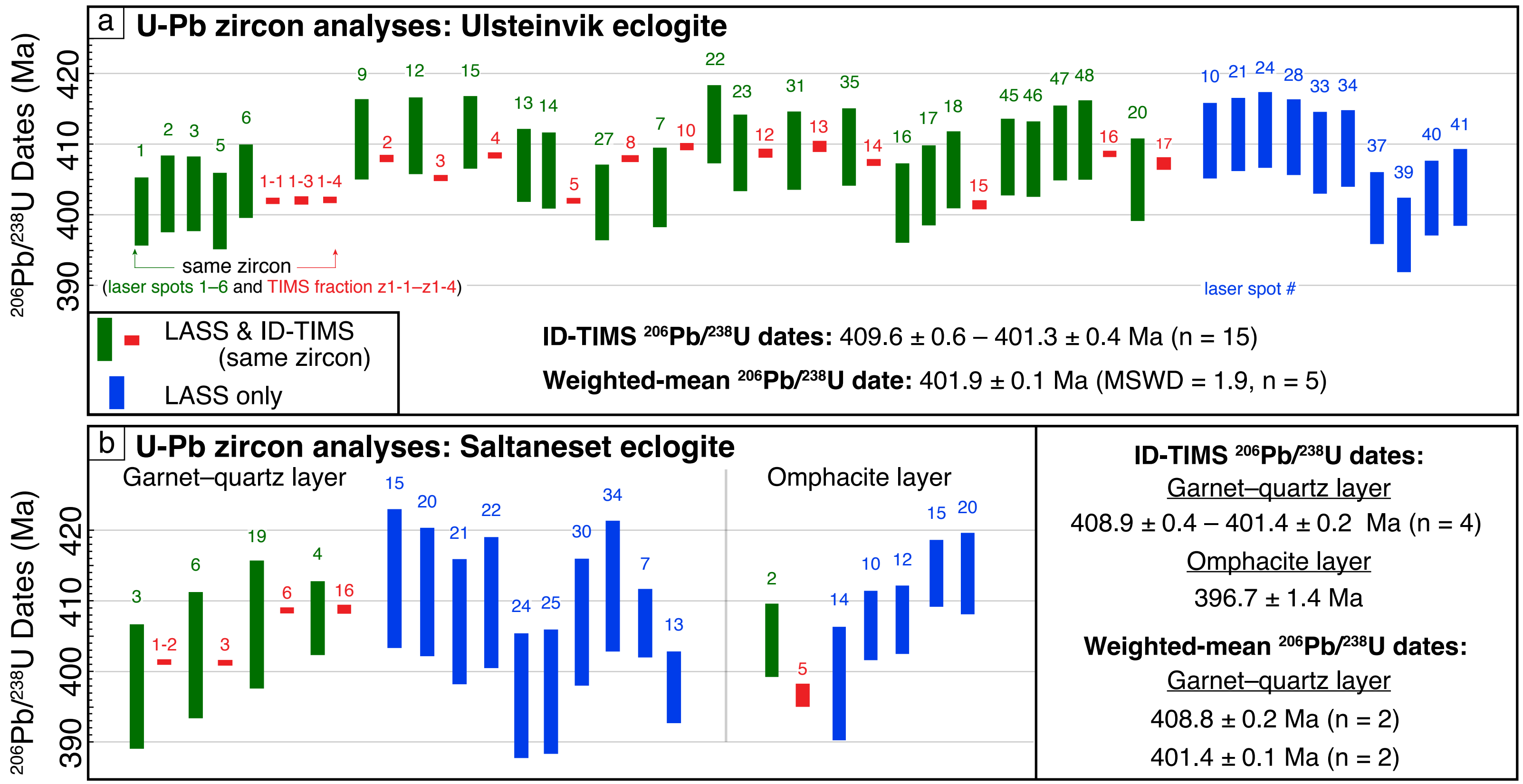

DesOrmeau et al. Figure 4

Figure 5

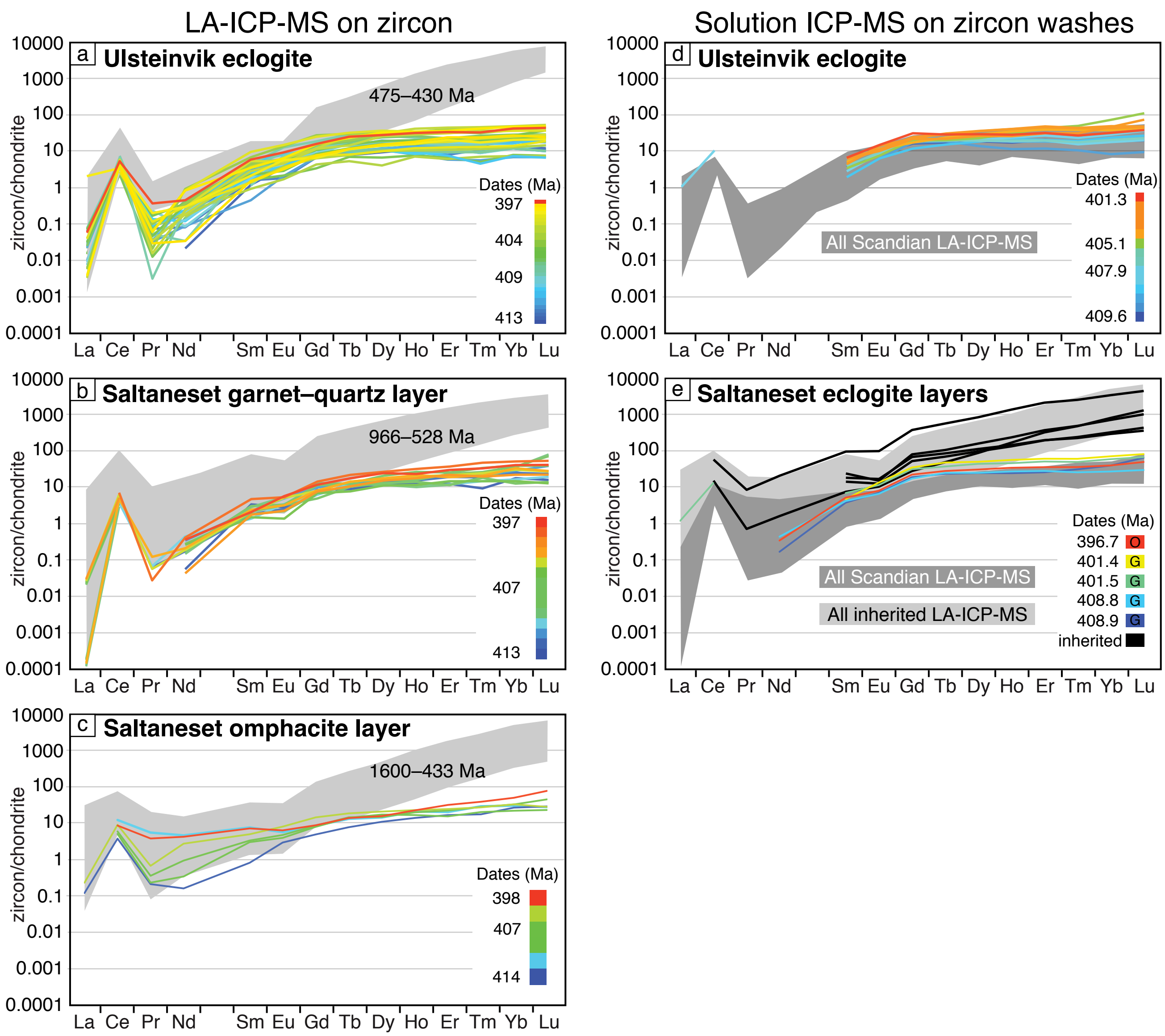

DesOrmeau et al. Figure 5

Figure 6

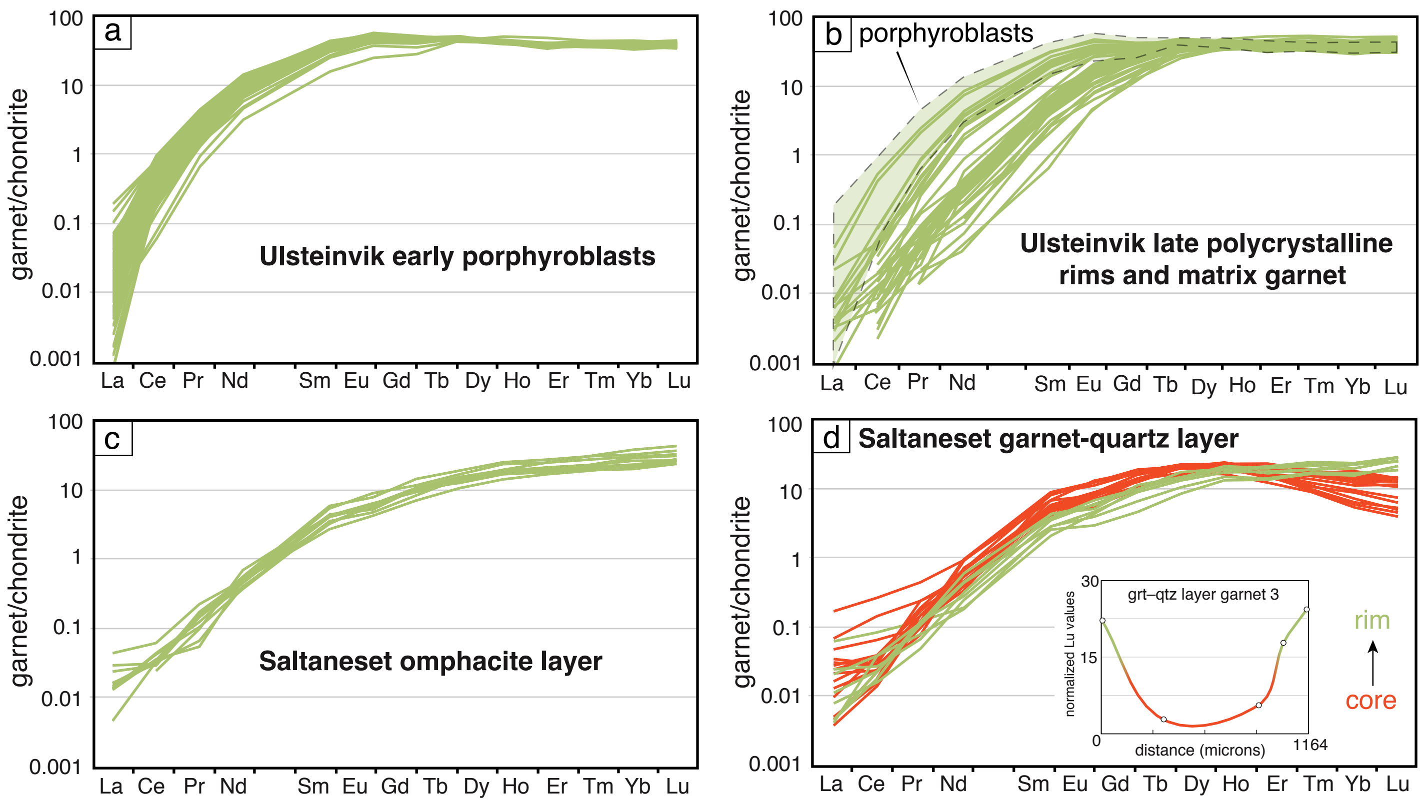

DesOrmeau et al. Figure 6

Figure 7

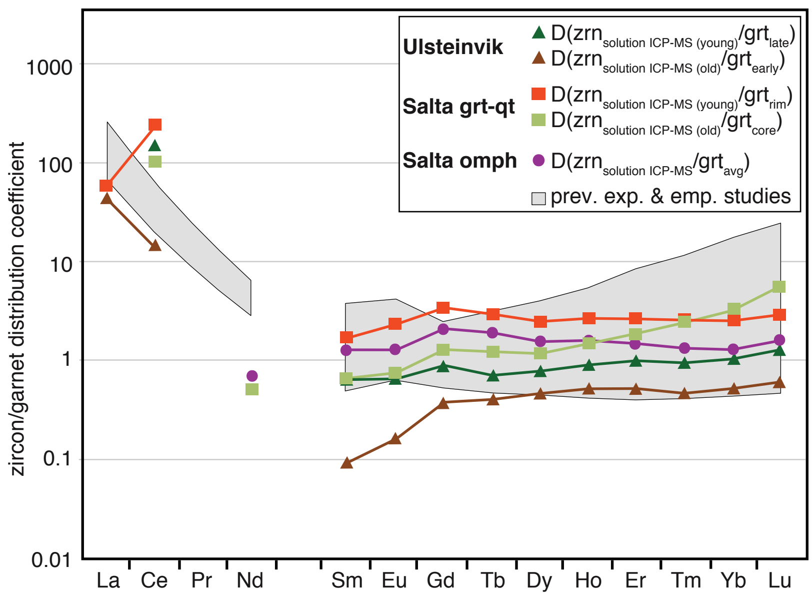

DesOrmeau et al. Figure 7

Figure S1

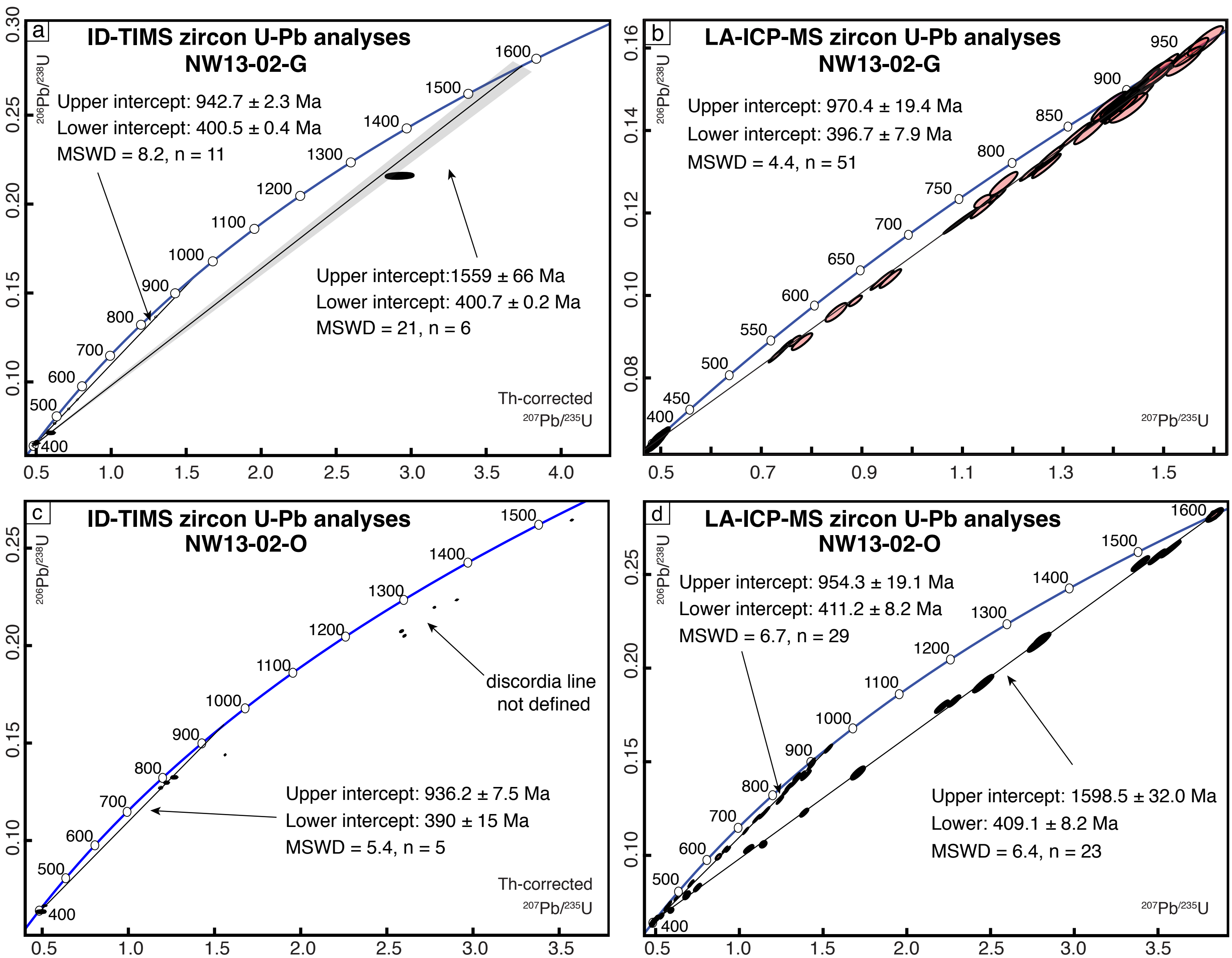

DesOrmeau et al. Figure S1

Figure S2

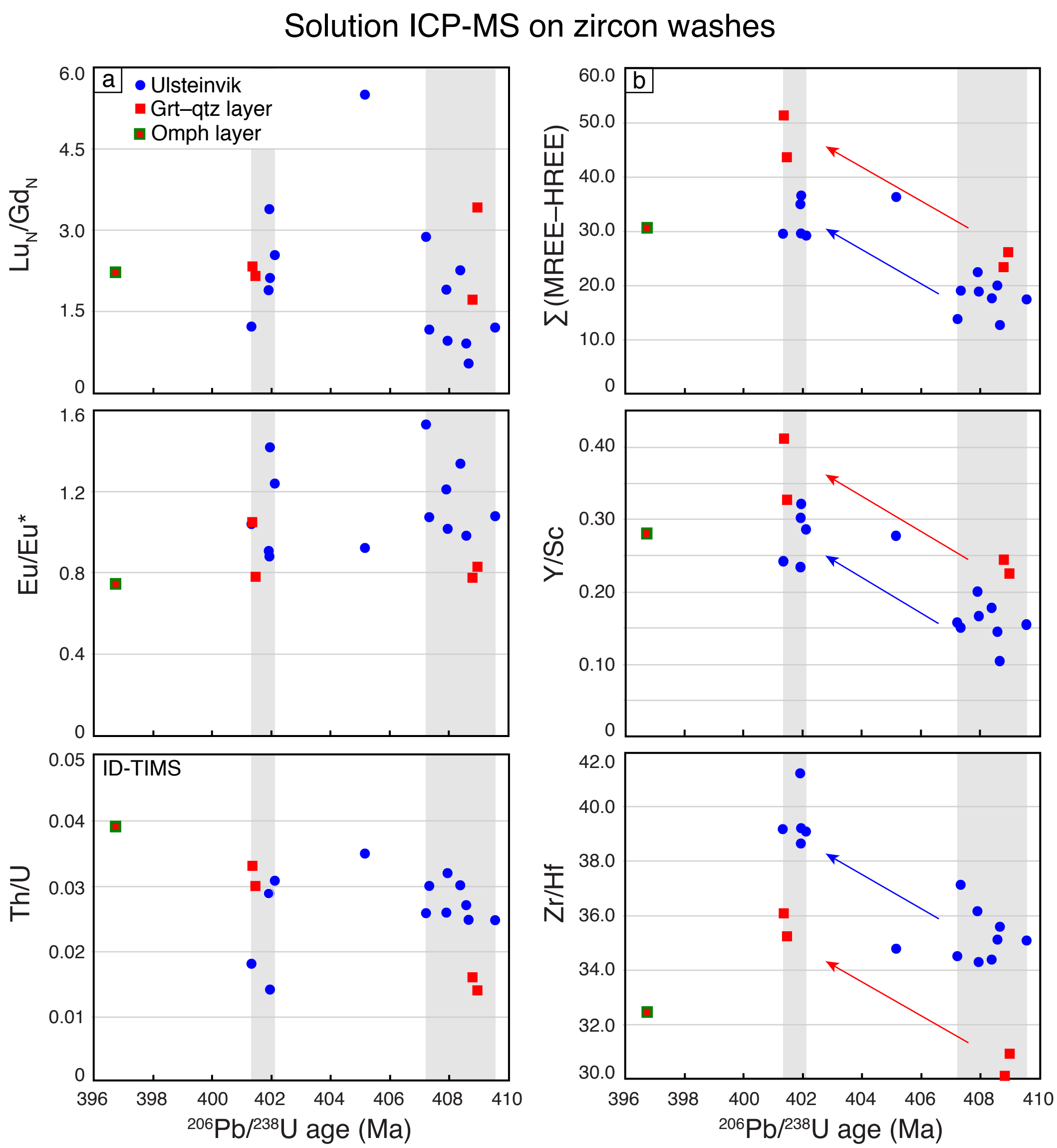

DesOrmeau et al. Figure S2

Figure S3

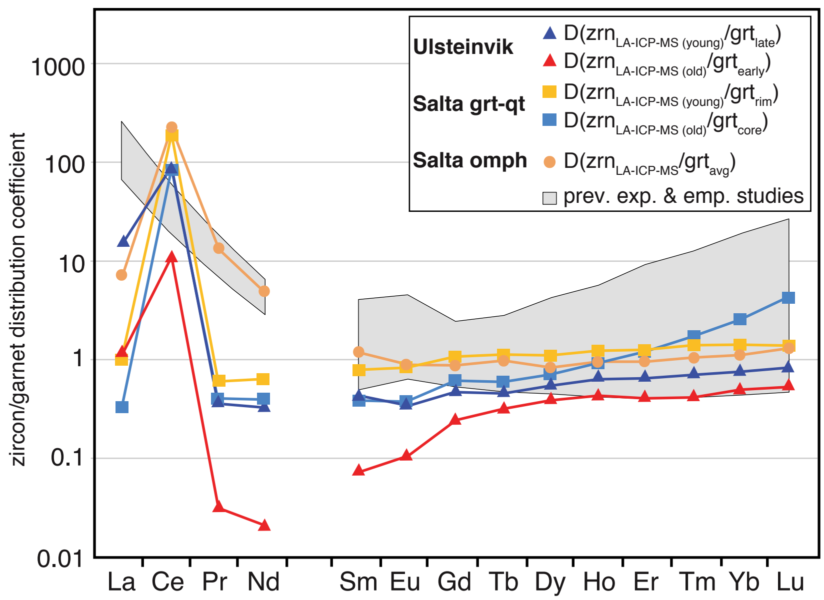

DesOrmeau et al. Figure S3

Table 1

Table 1

Geochronological summary of various Scandian (U)HP eclogites from the Western Gneiss Region

Sm-Nd isochron age (minerals), sample	**MSWD, n**	**location**
418 ± 11 Ma[1, 2] (grt-cpx), 1428; 418 ± 27 Ma' (grt-cpx)	*, n = 2	Tverrfjell (~15 km NE of Nordøyane)
423 ± 30 Ma[1, 2] (grt-cpx), N16; 422 ± 19 Ma' (grt-cpx)	*, n = 2	Ulsteinvik (Sorøyane)
423 ± 12 Ma[1, 2] (grt-cpx), 5/79; 423 ± 8 Ma' (grt-cpx)	*, n = 2	Vågsøy (Nordfjord)
407 ± 24 Ma[1, 2] (grt-cpx), K6; 407 ± 17 Ma' (grt-cpx)	*, n = 2	Frei (~45 km NE of Nordøyane)
408 ± 8 Ma[3] (w.r.-grt-cpx), 8067; 408 ± 6 Ma' (grt-cpx)	*, n = 3; *, n = 2	Almklovdalen (Nordfjord)
407 ± 76 Ma' (w.r.-grt-cpx)	MSWD = 3.7, n = 3	
400 ± 16 Ma[4] (w.r.-grt-cpx), EH13	*, n = 3	Flemsøya (Nordøyane)
410 ± 16 Ma' (w.r.-grt-cpx)	MSWD = 0.2, n = 3	
412 ± 12 Ma[5] (grt-cpx); 412 ± 4 Ma' (grt-cpx)	*, n = 2	Eiksunddal (Sorøyane)
408.3 ± 6.7 Ma[6] (w.r.-grt-cpx), Salt00-48	MSWD = 0.8, n = 3	Salta (Nordfjord)
402.7 ± 4.6 Ma[7] (w.r.-grt), R3703A2	*, n = 2	Vigra (~20 km SW of Nordøyane)
398.3 ± 5.5 Ma[7] (w.r.-grt-cpx), 9826J	MSWD = 2.0, n = 3	NW Gurskøy (~5 km S of Sorøyane)
388 ± 10 Ma[7] (w.r.-grt-cpx), 8815B	MSWD = 0.2, n = 3	Otrøy (Nordøyane)
384 ± 11 Ma[7] (w.r.-grt-cpx), 8906A11	MSWD = 1.4, n = 3	Remøya (Sorøyane)
397.1 ± 4.8 Ma[8] (w.r.-grt-cpx), P5701A	MSWD = 1.7, n = 4	Sandvik (Sorøyane)
398.3 ± 8.1 Ma[8] (w.r.-grt-cpx), E1612Q5	MSWD = 1.9, n = 4	Geiranger (southern edge of Nordfjord)
413.9 ± 3.7 Ma[8] (w.r.-grt-cpx), NOR205	MSWD = 0.5, n = 4	Gossa (Nordøyane)
393.4 ± 3.4 Ma[9] (grt-cpx), 8	*, n = 2	Svartberget (Nordøyane)
380.7 ± 5.7 Ma[9] (grt-cpx), 6	*, n = 2	
429.5 ± 3.1 Ma[10] (w.r.-grt-cpx), (DS0384, DS0380, Fl99-26)	*, n = 3	Otrøy and Flemsøy (Nordøyane)
Lu-Hf isochron age (minerals), sample		
419.5 ± 4.3 Ma[7] (w.r.-grt-cpx), 9901B1	MSWD = 1.8, n = 4	Verpeneset (Nordfjord)

Table 2

Table 2

Zircon U-Th-Pb LA-ICP-MS isotopic data from the Western Gneiss Region: Ulsteinvik and Saltaneset eclogites

	Composition			**Isotopic Ratios**			
	Approx. U (ppm)	Approx. Th (ppm)	Th/U	$^{207}Pb/^{235}U$	±2σ abs	$^{206}Pb/^{238}U$	±2σ abs
LA-ICP-MS results for Ulsteinvik and Saltaneset eclogite garnet-quartz and omphacite layers dated by ID-TIMS							
8815E, Ulsteinvik							
Sample, Laser spot number, ID-TIMS zircon fraction							
Ulsteinvik_1_z1-1	280	7	0.03	0.480	0.007	0.0641	0.0008
Ulsteinvik_2_z1-3	330	10	0.03	0.487	0.008	0.0645	0.0009
Ulsteinvik_3_z1-4	416	14	0.03	0.487	0.007	0.0645	0.0008
Ulsteinvik_5_z1	263	9	0.03	0.484	0.008	0.0641	0.0009
Ulsteinvik_6_z1	269	10	0.04	0.492	0.007	0.0648	0.0008
Ulsteinvik_9_z2	246	7	0.03	0.496	0.008	0.0658	0.0009
Ulsteinvik_12_z3	243	6	0.03	0.499	0.007	0.0659	0.0009
Ulsteinvik_15_z4	258	7	0.03	0.498	0.007	0.0659	0.0008
Ulsteinvik_13_z5	437	8	0.02	0.497	0.007	0.0652	0.0008
Ulsteinvik_14_z5	413	5	0.01	0.490	0.007	0.0651	0.0009
Ulsteinvik_27_z8	193	3	0.02	0.488	0.008	0.0643	0.0009
Ulsteinvik_7_z10	195	6	0.03	0.495	0.009	0.0647	0.0009
Ulsteinvik_22_z12	297	9	0.03	0.504	0.008	0.0661	0.0009
Ulsteinvik_23_z12	391	16	0.04	0.502	0.007	0.0654	0.0008
Ulsteinvik_31_z13	239	6	0.03	0.494	0.008	0.0655	0.0009
Ulsteinvik_35_z14	252	8	0.03	0.493	0.008	0.0656	0.0009
Ulsteinvik_16_z15	511	11	0.02	0.484	0.007	0.0643	0.0009
Ulsteinvik_17_z15	523	11	0.02	0.489	0.007	0.0647	0.0009
Ulsteinvik_18_z15	373	6	0.02	0.494	0.007	0.0651	0.0009
Ulsteinvik_45_z16	413	15	0.04	0.496	0.007	0.0654	0.0009
Ulsteinvik_46_z16	263	7	0.03	0.498	0.008	0.0653	0.0009

Table 3

Table 3

Zircon U-Pb ID-TIMS isotopic data from the Western Gneiss Region: Ulsteinvik and Saltaneset eclogites

				Composition	
Sample	location[a]	mineral assemblage[b]	Fraction	Pb*/ Pbc [h]	Pb* (pg) [f]
8815E-Ulsteinvik	32V 337447 6915556	Omp, Grt, Aug,	z1-1	366	68
		Pl, Qz, Amp, Bt,	z1-3	48	8
		Rt, Zrn	z1-4	481	214
			z2	73	13
			z3	80	14
			z4	49	11
			z5	110	20
			z8	87	14
			z10	56	10
			z12	25	4
			z13	23	5
			z14	19	45
			z15	11	25
			z16	53	139
			z17	6	14
NW13-02-G	32V 308668 6882327	Qz, Grt, Rt, Zr	z1-1	394	109
Saltaneset garnet–quartz layer			z1-2	682	194
			z2-1	573	187
			z2-2	315	54
			z3	72	21
			z5-1	177	23
			z6	39	30
			z7	26	4
			z9	461	90
			z11	60	10
			z14	4	8
			z15	3	7
			z16	11	24
NW13-02-O	32V 308668 6882327	Omp, Grt, Qz,	z1-3	583	98
Saltaneset omphacite layer		Pl, Amp,Rt, Zrn	z1-4	238	74
			z2	382	116
			z3-2	97	21
			z4-1	137	19
			z4-3	83	15

Table 4

Table 4

Chondrite normalized zircon LASS and solution ICP-MS trace-element data from the Western Gneiss Region: Uls

Zircons analyzed by ID-TIMS and LASS	La	Ce	Pr
Ulsteinvik-8815E, eclogite			
Ulsteinvik_ z1_1	bdl	3.8	0.03
Ulsteinvik_ z1_2	bdl	4.7	0.04
Ulsteinvik_z1_3	0.003	6.0	0.02
Ulsteinvik_z1_5	0.004	4.2	0.1
Ulsteinvik_z1_6	bdl	3.8	0.1
Ulsteinvik_z2_9	0.02	3.9	0.04
Ulsteinvik_z3_12	0.06	3.3	0.03
Ulsteinvik_z4_15	0.02	3.5	0.1
Ulsteinvik_z5_13	0.03	4.8	0.1
Ulsteinvik_z5_14	0.07	4.3	0.05
Ulsteinvik_z8_27	bdl	2.8	0.1
Ulsteinvik_z10_7	0.02	2.7	0.1
Ulsteinvik_z12_22	0.01	4.9	bdl
Ulsteinvik_z12_23	0.03	6.8	0.003
Ulsteinvik_z13_31	0.01	3.9	bdl
Ulsteinvik_z14_35	0.03	3.6	0.1
Ulsteinvik_z15_16	0.04	5.7	0.1
Ulsteinvik_z15_17	0.01	5.5	0.02
Ulsteinvik_z15_18	0.03	4.1	0.2
Ulsteinvik_z16_45	bdl	7.6	0.1
Ulsteinvik_z16_46	bdl	4.4	bdl
Ulsteinvik_z16_47	bdl	4.6	0.1
Ulsteinvik_z16_48	bdl	4.5	0.1
Ulsteinvik_z17_20	0.02	2.4	0.01
NW13-02-G, Saltaneset eclogite (garnet-quartz layer)			
NW13_02_grt_z1_3	0.03	5.4	bdl
NW13_02_grt_z3_6	0.03	6.6	0.1
NW13_02_grt_z6_19	0.02	4.4	bdl
NW13_02_grt-z16_4	0.0001	3.0	bdl
NW13-02-O, Saltaneset eclogite (omphacite layer)			
NW13_02_omph_z5_2	0.2	9.4	0.7
Zircons analyzed by LASS			
Ulsteinvik-8815E, eclogite			
Ulsteinvik_10	bdl	4.7	bdl

Table 5

Table 5

Chondrite normalized garnet LA-ICP-MS trace-element data and calculated zircon-garnet partition coefficients fı

***In situ* garnet analyses**	La	Ce	Pr
8815E, Ulsteinvik eclogite			
garnet 1 8815E-low-1	0.07	0.3	1.3
8815E-low-2	0.04	0.4	2.3
8815E-low-3	0.02	0.4	2.3
8815E-low-4	0.02	0.4	2.1
8815E-low-5	0.02	0.3	1.9
8815E-low-6	0.02	0.2	1.6
8815E-low-7	0.02	0.4	2.2
8815E-low-8	0.02	0.4	2.4
8815E-low-9	0.04	0.5	2.3
8815E-low-10	0.03	0.5	2.9
8815E-low-11	0.02	0.4	2.5
8815E-low-12	0.03	0.4	2.5
8815E-low-13	0.02	0.5	2.6
8815E-low-14	0.04	0.5	3.1
8815E-low-15	0.02	0.5	3.2
8815E-low-16	0.02	0.5	2.9
8815E-low-17	0.03	0.5	3.1
8815E-low-18	0.1	0.8	3.6
8815E-low-19	0.02	0.6	3.3
8815E-low-20	0.03	0.6	3.3
8815E-low-21	0.03	0.6	3.3
8815E-low-22	0.06	0.7	3.5
8815E-low-23	0.05	0.6	3.5
8815E-low-24	0.1	0.8	4.1
8815E-low-25	0.05	0.8	3.8
8815E-low-26	0.05	0.7	3.8
8815E-low-28	0.06	0.7	3.6
8815E-low-29	0.04	0.7	3.5
8815E-low-30	0.03	0.5	2.7
8815E-low-31	0.07	0.6	2.6
8815E-low-32	0.05	0.6	3.2
8815E-low-33	0.06	0.6	2.6
8815E-low-34	0.03	0.4	1.8
8815E-low-35	0.02	0.2	1.4
8815E-low-36	0.03	0.3	1.9
8815E-low-37	0.03	0.4	2.5